# Supplementary information for

# Vibration suppression mechanism of ultrasonic field energy

**Authors:** Lianjun Sun[1], Wenhe Liao[1*], Kan Zheng[1*], Song Dong[1], Wei Tian[2], Zhenwen Sun[1], Jing Shu[1]& Feng Xue[1]

**Affiliations:**
[1]School of Mechanical Engineering, Nanjing University of Science and Technology, Nanjing 210094, P.R. China.
[2]College of Mechanical and Electrical Engineering, Nanjing University of Aeronautics and Astronautics, Nanjing 210016, P.R. China.

[*]Corresponding authors. Email:
cnwho@njust.edu.cn (WL)
zhengkan@njust.edu.cn (KZ)

**This supplementary file includes:**

Supplementary Method
Supplementary Results
Supplementary Figs. S1 to Supplementary Figs. S26
Supplementary Table S1 to Supplementary Table S6
References

**Other supplementary information for this manuscript includes the following:**

Supplementary Excel S1 and Supplementary Excel S2

# Supplementary Methods

## Constructing intrinsic relationship model

In this paper, an energy ratio ($\gamma_v$) is introduced and the intrinsic relationship expression can be written as:

$$E_u = \gamma_v E_v \tag{S1}$$

It can be found that the parameter $\gamma_v$ is the bridge between ultrasonic energy field and vibration energy field. The energy ratio $\gamma_v$ can be defined as:

$$\gamma_v = \frac{E_{uc}}{E_{vc}} \tag{S2}$$

Among them, the $E_{uc}$ denotes a certain ultrasonic energy field; $E_{vc}$ is the largest vibration energy field that $E_{uc}$ can suppress. Therefore, the characterization of $E_u$ and calculation of $\gamma_v$ are the key to construct the relationship model.

### 1.Characterizing ultrasonic energy field

During a quarter of a cycle of ultrasonic energy wave, the product of work (done by the ultrasonic generator) and the energy conversion efficiency of ultrasonic machining system is the kinetic energy of ultrasonic energy field. According to the energy conservation law, the ultrasonic field energy ($E_u$) can be expressed as:

$$\begin{aligned} E_u &= \frac{1}{2} M_{\mathrm{e}} V_L^2 + \frac{1}{2} M_e V_T^2 \\ &= \frac{1}{4} P_{el} T \eta_u \end{aligned} \tag{S3}$$

Where the $V_L$ and $V_T$ are the longitudinal and torsional vibration velocity of ultrasonic vibration, respectively. The $M_e$ is the effective mass of tool. $T$ is the ultrasonic vibration period. The energy conversion efficiency ($\eta_u$) of ultrasonic machining system can be calculated by the ratio of actual result to theoretical design value:

$$\eta_u = \frac{E_u}{E_d} = \frac{V_L^2 + V_T^2}{\left(V_L^d\right)^2 + \left(V_T^d\right)^2} \tag{S4}$$

Where the $d$ represents the theoretical design values of ultrasonic machining system parameters. In this study, the value of $\eta_u$ is 50.65%.

Since the value of $M_e$ is difficult to determine, the ultrasonic field energy can be characterized by the power $P_{el}$. Thus, the relationship model of ultrasonic field energy and vibration field energy can be further expressed as

$$\frac{1}{4} P_{el} T \eta_u = \gamma_v E_v \tag{S5}$$

A simplification of Eq. (S5) can be expressed as the Eq. (5). Among them, the correlation coefficient $k_v$ in Eq. (5) can be written as:

$$k_v = \frac{4\gamma_v}{\eta_u} \tag{S6}$$

It can be found that the $k_v$ is related to energy conversion efficiency of ultrasonic machining system ($\eta_u$) and vibration suppression capability of ultrasonic energy field ($\gamma_v$). The $\gamma_v$ is affected by the distribution law of external excitation field itself. The effect of ultrasonic energy field on vibration suppression is not the same under different excitation fields (or cutting energy fields) such as milling, drilling, grinding and boring. Since the $\eta_u$ has been determined, taking the milling as example, it is necessary to provide a method for calculating the energy ratio $\gamma_v$.

## 2.Calculating energy ratio

The energy ratio $\gamma_v$ showing the vibration suppression ability of ultrasonic energy field can be calculated by the Eq. (S2). Among them, the $E_{uc}$ has been achieved based on Eq. (S3). Next, a method is proposed to calculate the $E_{vc}$ under the effect of ultrasonic energy field ($E_{uc}$). During stability analysis, the machining system is usually equivalent to a mass-spring-damping system[1]. According to mechanism analysis, the vibration energy is maintained in a steady state after the transition phase. Thus, for RUMC-LT, the Eq. (3) can be further expressed as:

$$E_v = 2\pi^2\left(\sum_{u=1}^{m_e} m_{RMS,u}\, p_{RMS,u}^2 Q_{RMS,u}^2 + \sum_{u=1}^{n_e} m_{CMS,u}\, p_{CMS,u}^2 Q_{CMS,u}^2\right) \tag{S7}$$

Where $m_{RMS,u}$ and $m_{CMS,u}$ denote the modal mass of RMS and CMS, respectively. $P_{RMS,u}$ and $P_{CMS,u}$ are natural frequency of machining system; In the case of robotic milling rigid components, $E_{RCM}$ is only determined by the robotic chatter energy; $m_e$ and $n_e$ represents the number of modes in which chatter occurs. It's worth noting that the instability process of robot and component is from single mode to multiple modes with the increasing of self-excited vibration energy as shown in Fig. 3. Thereby, the $m_e$ and $n_e$ should be all the modes with chatter while the stable modes are excluded.

As presented in Fig. 5a, stability boundary curve is a common method to study the vibration characteristic of machining system. For RUMC-LT, the processing parameter on this boundary curve represents the maximum of stability cutting depth on the basis of a given ultrasonic energy field ($E_{uc}$). The machining system occurs vibration phenomenon when the machining parameters are above this curve. The critical cutting depth means the limit of ultrasonic energy field to suppress vibration. Under this critical parameter, the RUMC-LT system is bound to vibrate when the ultrasonic energy field value is zero. At this time, the vibration energy of machining system is the maximum value that ultrasonic energy field can suppress. It is called $E_{vc}$. Thus, the calculation process of $\gamma_v$ includes the following four steps:

(1) According to the mechanism analysis, the RUMC-LT stability boundary curve can be drawn with a certain ultrasonic energy field ($E_{uc}$).

(2) Let the ultrasonic field energy be zero. By the machining parameters on boundary curve, the vibration amplitude ($Q_{RMS}$ and $Q_{CMS}$) of machining system is calculated based on vibration energy accumulation effect.

(3) The value of $E_{vc}$ is obtained by taking the vibration amplitudes into Eq. (S7).

(4) The value of $\gamma_v$ can be calculated by Eq. (S2) based on the $E_{vc}$ and $E_{uc}$.

It can be found that the vibration energy field ($E_{vc}$) is the key to determining the parameter $\gamma_v$. Its accuracy is related to RUMC-LT stability boundary curve. The calculation value of $\gamma_v$ is 0.00042 based on the point 6 in Fig. 5a.

Based on the experimental platform described in main text, the measurement expression of $k_v$ (or $\gamma_v$) value can be written as:

$$\gamma_v^e = \frac{E_u}{E_v\left(u=0\right) - E_v(u)} \tag{S8}$$

$$k_v^e = \frac{4\gamma_v^e}{\eta_u} \tag{S9}$$

Where $E_v(u=0)$ represents the vibration energy of machining system without ultrasonic energy field; $E_v(u)$ is the vibration energy of machining system under the effect of ultrasonic energy field ($E_u$). Their values are obtained by the Eq. (S7) on the basis of robotic milling signals. Moreover, the accuracy of $k_v$ ($k_v$=0.0033) can be expressed as:

$$A_c\left(N\right) = 1 - \frac{\left|\frac{1}{N}\sum_{i=1}^{N} k_v^e\left(i\right) - k_v\right|}{k_v} \left(N = 1,2,3...\right) \tag{S10}$$

Where the parameter $N$ is the experiment groups (or sample size). Finally, the experimental results of accuracy are presented in Fig. 5e with the $N$ from 1 to 100.

**Stability boundary curve and energy accumulation effect**

**1. RUMC-LT dynamic behavior**

In this paper, the stability curve is investigated to verify the previous inhibition mechanism and construct relationship model of energy fields. According to the previous mechanism analysis about energy fields coupling, with the increasing of cutting depth, RUMC-LT instability process includes three stages:

(1) Stage one: RMS and CMS are both stable. In this stage, the cutting depth of RUMC-LT is small. The input energy under the action of energy fields coupling can be completely consumed by damping. Thus, the dynamic expression can be written as:

$$\left[M_f\right]\ddot{Q}_f + \left[C_f + C_p\right]\dot{Q}_f + \left[K_f\right]Q = \left[dF_f\right] \quad (f\text{=RMS, CMS}) \tag{S11}$$

Where the process damping ($C_p$) can be calculated according to the study of Ahmadi and Altintas[2]. The Eq. (S11) denotes the dynamic equation of RMS when the $f$ is $R$. Otherwise, it is the dynamic expression of CMS. In stage one, the RMS and CMS could be viewed as independent of each other since they are both stable. The critical instability curve corresponding to this stage is named $RC_{sc}$. It means that RMS or CMS occurs vibration when cutting depth parameter is above this curve.

(2) Stage two: Single machining system (RMS or CMS) occurs instability. As the growth of cutting depth exceeds the curve $RC_{sc}$, it makes energy generation rate exceed consumption rate. At this time, one of the RMS and CMS appears chatter due to the

difference in their dynamics. In this condition, for RMCS with RMS and CMS, the following definitions are made as:

$$\begin{cases} R/\mathrm{C} & = & RMS & or & CMS \\ C/R & = & CMS & or & RMS \\ R/C+C/R & = & RMS & + & CMS \end{cases} \tag{S12}$$

Then, RUMC-LT dynamic can be expressed as:

$$M_f\ddot{Q}_f(t)+\left[C_f+C_p\right]\dot{Q}_f(t)+K_fQ_f(t)=dF_f(t) \quad f=\left(R/C \ or \ C/R\right) \tag{S13}$$

In stage two, the self-excited vibration energy of single system begins to accumulate. When the energy generation rate is equal to dissipation rate, the vibration energy is maintained in a constant state. At this time, its vibration amplitude and frequency can be applied for calculating the Eq. (S7).

(3) Stage three: RMS and CMS are both unstable. As the cutting depth continues to increase, both the RMS and CMS occur vibration phenomenon above the curve $R_cW_c$ in Fig. 5a. In this case, the dynamic expressions can be displayed as:

$$M_f\ddot{Q}_f(t)+\left[C_f+C_p\right]\dot{Q}_f(t)+K_fQ_f(t)=dF_f(t) \quad f=\left(RMS \ and \ CMS\right) \tag{S14}$$

The vibration vector $Q_f(t)$ can be calculated by the modal displacement vector $\Gamma_f(t)$:

$$Q_f(t)=U_f\cdot\Gamma_f(t) \tag{S15}$$

Among them, $U_f$ is the mass normalized mode shape matrix. The following expression can be written as:

$$U_f^T\cdot M_f\cdot U_f=I_f \tag{S16}$$

$$U_f^T\cdot K_f\cdot U_f=\omega_f^2 \tag{S17}$$

Then, the dynamic equation could be expressed as:

$$\ddot{\Gamma}_f(t)+\left[2\left(\zeta_f+\zeta_p\right)\omega_f\right]\dot{\Gamma}_f(t)+\omega_f^2\Gamma_f(t)=U_f^TdF_f(t) \tag{S18}$$

Where the $\zeta_f$ is the modal damping ratio, and the $2\zeta_f\omega_f$ can be obtained by the Rayleigh damping theory[3] as:

$$2\left(\zeta_f+\zeta_p\right)\omega_f=\alpha_f\cdot I_f+\beta_f\cdot\omega_f^2 \tag{S19}$$

Due to the energy fields coupling of RMS and CMS, the energy accumulation rate grows as the cutting depth continues to increase in stage three. When the energy generation rate is equal to dissipation rate, the vibrational energy is maintained in a constant state. At this time, its vibration amplitude and frequency can be applied for calculating the Eq. (S7).

## 2.Cutting energy field under the action of $E_u$

Based on the mechanism analysis, the addition of ultrasonic field energy changes direction and frequency of cutting energy field. Then, the magnitude of cutting energy field is reduced. As a result, the dynamic milling force ($dF_f$) which denotes the important input parameter of dynamic expression is also decreased. On the one hand, for the direction variation of cutting energy field, its effect on $dF_f$ can be calculated by introducing the ultrasonic function angles. On the other hand, the increasing of contact frequency between tool and workpiece which weakens the cutting energy field could be characterized by the separation characteristic of ultrasonic energy field. In this study, the ultrasonic energy field possesses separation effect when the spindle speed range is from 2000r/min to 3200r/min (Fig. 5a). According to the study of Ding et al.[4] and Insperger et al.[5], the stability boundary curve and vibration energy can be achieved as presented in Fig. 5a. The specific calculation process is presented as follow:

As presented in Supplementary Fig. S1, with the increasing of cutting depth, the instability process of RUMC-LT includes three stages: RMS and CMS are both stable, the machining chatter occurs in RMS or CMS, both RMS and CMS are unstable.

**2.1Stage one: RMS and CMS are both stable**

The dynamic chip thickness ($dh_f$) under the effect of ultrasonic field energy could be expressed as[6]:

$$dh_f = \left[\left(Q_{f,x}\cdot\sin\phi_j + Q_{f,y}\cdot\cos\phi_j\right)\cdot\sin\gamma - Q_{f,z}\cdot\cos\gamma\right]\cdot\sin\alpha \quad \text{(S20)}$$

Among them, $Q_{f,x}$, $Q_{f,y}$ and $Q_{f,z}$ represent the dynamic displacement along the three coordinate directions of RMS and CMS; $\phi_j$ is the rotation angle of tooth $j$; $\alpha$ and $\gamma$ are the ultrasonic function angles[6].

The dynamic milling forces ($dF_f$) of RUMC-LT can be written as:

$$\begin{bmatrix} dF_{f,x} \\ dF_{f,y} \\ dF_{f,z} \end{bmatrix} = \Psi\cdot\left[b\cdot C(t) + A\cdot D(t)\right]\cdot\begin{bmatrix} Q_{f,x} \\ Q_{f,y} \\ Q_{f,z} \end{bmatrix} \quad \text{(S21)}$$

Where $\Psi$ denotes the type of ultrasonic milling[6]. The RUMC-LT is separated when the value of $\Psi$ is less than one. Otherwise, it is unseparated. $A$ is the amplitude of longitudinal ultrasonic vibration. $C(t)$ and $D(t)$ are coefficient matrixes under the effect of ultrasonic field energy[6].

Based on the dynamic equation in Eq. (S11) and combined with second-order full-discretization method (FDM)[4], the stability lobe diagrams (SLDs) could be achieved by the single mode. According to the Floquet theory, the corresponding chatter frequency ($p$) could be calculated with the characteristic multiplier $\mu(a,b)$ as[5]:

$$p(a,b) = \pm\frac{\mathrm{Im}\left[\ln\mu(a,b)\right]}{2\pi T} + \frac{l\cdot a}{60} \quad l = 0, \pm1, \pm2, .... \quad \text{(S22)}$$

Among them, the parameter $T$ is the time period of FDM; $a$ represents the spindle speed.

Nevertheless, the robotic milling stability is influenced by multiple modes of the low stiffness machining system according to the study of Sun et al.[7] and Cordes et al[8]. In this paper, the matrixes $\Phi_{RMS}$ and $\Phi_{CMS}$ are the first $m$-order (or $n$-order) modes of RMS and CMS as:

$$\phi_{RMS} = \begin{bmatrix} \phi_{RMS,1} & \phi_{RMS,2} & \cdots & \phi_{RMS,m} \end{bmatrix} \tag{S23}$$

$$\phi_{CMS} = \begin{bmatrix} \phi_{CMS,1} & \phi_{CMS,2} & \cdots & \phi_{CMS,n} \end{bmatrix} \tag{S24}$$

The initial robotic pose and modes are shown in Supplementary Table S1, Supplementary Table S2 and Supplementary Table S3. Finally, the stability boundary curve is presented in Supplementary Fig. S2.

### 2.2 Stage two: The machining chatter occurs in RMS or CMS

In stage two, one of the RMS and CMS appears machining vibration and the self-excited vibration energy begins to accumulate in single machining system. The accumulation of self-excited vibration energy and ultrasonic field energy in *i*-th mode could be expressed as:

$$E_v^{R/C} = 2\pi^2 \sum_{u=1}^{m_e} m_{RMS,u}\, p_{RMS,u}^2 Q_{RMS,u}^2 \ \ or\ \ 2\pi^2 \sum_{u=1}^{n_e} m_{CMS,u}\, p_{CMS,u}^2 Q_{CMS,u}^2 \tag{S25}$$

It is worth noting that $Q_{RMS,u}$ and $Q_{CMS,u}$ represent the energy value when the vibration reaches a constant state. At this time, the vibration keeps unchanging. According to the Duhamel integral formula, the $Q_{R/C,u}$ of *k*-th self-excited vibration energy in Fig. 1 can be expressed as:

$$\begin{aligned} Q_{R/C,u}(a,b,k) &= \frac{dF_{R/C,u}(a,b,k\text{-}1)}{K_{R/C,k}} \\ &= E + e^{-\frac{\xi_{R/C,u}\omega_{R/C,u}}{p_{R/C,u}(a,b)}} \left[ \alpha_{R/C} \cdot \sin\left( \frac{\bar{\omega}_{R/C,u}}{p_{R/C,u}(a,b)} \right) + \beta_{R/C} \cdot \cos\left( \frac{\bar{\omega}_{R/C,u}}{p_{R/C,u}(a,b)} \right) \right] \end{aligned} \tag{S26}$$

$$\begin{aligned} E = \frac{1}{\bar{\omega}_{R/C,u}} \int_0^{\frac{1}{p_{R/C,u}(a,b)}} dF_{R/C,u}(a,b,k-1,\tau) \cdot e^{-\omega_{R/C,u}\xi_{R/C,u}\left(\frac{1}{p_{R/C,u}(a,b)}-\tau\right)} \\ \cdot \sin \bar{\omega}_{R/C,u} \left( \frac{1}{p_{R/C,u}(a,b)} - \tau \right) d\tau \end{aligned}$$

Among them,

$$\bar{\omega}_{R/C,u} = \omega_{R/C,u} \sqrt{1-\left(\zeta_{R/C,u}+\zeta_p\right)^2} \tag{S27}$$

$$\xi_{R/C,u} = \frac{\alpha_{R/C} + \beta_{R/C}\omega_{R/C,u}^2}{2\omega_{R/C,u}} \tag{S28}$$

Where the $\alpha_{R/C}$ and $\beta_{R/C}$ are the Duhamel integral constant. They can be calculated by the Rayleigh damping theory[3]. The $K_{f,k}$ is the processing stiffness of *k*-th vibration which can be obtained by the Eq. (S29).

According to the Eq. (3), the vibration energy accumulation is a coupling process of dynamic milling force and displacement. It is assumed that the RMS (or CMS) vibrates $k$ times during the time $t_e$, the coupling of force and displacement can be expressed as:

$$
\begin{aligned}
dF_{R/C,u}(a,b,0) &= \Psi\cdot\sum_{j=1}^{N_e}\chi(j)\cdot Q_{R/C,u}(a,b,0)\\
dF_{R/C,u}(a,b,1) &= \Psi\cdot\sum_{j=1}^{N_e}\chi(j)\cdot\frac{dF_{R/C,u}(a,b,0)}{K_{R/C,1}}\\
&= \Psi\cdot\sum_{j=1}^{N_e}\chi(j)^2\cdot\frac{1}{K_{R/C,1}}\cdot Q_{R/C,u}(a,b,0)\\
dF_{R/C,u}(a,b,2) &= \Psi\cdot\sum_{j=1}^{N_e}\chi(j)\cdot\frac{dF_{R/C,u}(a,b,1)}{K_{R/C,2}}\\
&= \Psi\cdot\sum_{j=1}^{N_e}\chi(j)^3\cdot\frac{1}{K_{R/C,1}\cdot K_{R/C,2}}\cdot Q_{R/C,u}(a,b,0)\\
&\cdots\cdots\\
dF_{R/C,u}(a,b,k) &= \Psi\cdot\sum_{j=1}^{N_e}\chi(j)\cdot\frac{dF_{R/C,u}(a,b,k\text{-}1)}{K_{R/C,k}}\\
&= \Psi\cdot\sum_{j=1}^{N_e}\chi(j)^{k+1}\cdot\frac{1}{K_{R/C,1}\cdot K_{R/C,2}\cdots K_{R/C,k}}\cdot Q_{R/C,u}(a,b,0)
\end{aligned}
\tag{S29}
$$

Among them, the $\chi(j)$ can be expressed as $\chi(j)=bC(t)+AD(t)$; $N_e$ is the cutting teeth number; $dF_{R/C,u}(a,b,0)$ and $Q_{R/C,u}(a,b,0)$ is the initial value determined by the $\chi(j)$. The $C_e(t)$ and $D_e(t)$ are the energy accumulation coefficient matrixes under the effect of ultrasonic field energy[6]. It could be expressed as:

$$
C_e(t)=\begin{bmatrix}\alpha_{xx} & \alpha_{xy} & \alpha_{xz}\\ \alpha_{yx} & \alpha_{yy} & \alpha_{yz}\\ \alpha_{zx} & \alpha_{zy} & \alpha_{zz}\end{bmatrix}\ \text{and}\ D_e(t)=\begin{bmatrix}\beta_{xx} & \beta_{xy} & \beta_{xz}\\ \beta_{yx} & \beta_{yy} & \beta_{yz}\\ \beta_{zx} & \beta_{zy} & \beta_{zz}\end{bmatrix}
\tag{S30}
$$

Among them, $D_e(t)=\sin(2\pi f_{va}t)C_e(t)$. $f_{va}$ is the ultrasonic vibration frequency along the axial direction. The nine elements in matrix $C_e(t)$ could be written as:

$$\alpha_{xx}=g(\phi_j)\cdot q\cdot(h_s)^{q-1}\cdot(-ss_1s_2)\cdot\left[K_r\cdot(ss_1s_2+cc_1)+K_t\cdot c+K_a\cdot sc_2\right]$$

$$\alpha_{xy}=g(\phi_j)\cdot q\cdot(h_s)^{q-1}\cdot(cs_1s_2)\cdot\left[K_r\cdot(ss_1s_2+cc_1)+K_t\cdot c+K_a\cdot sc_2\right]$$

$$\alpha_{xz}=g(\phi_j)\cdot q\cdot(h_s)^{q-1}\cdot(-s_1c_2)\cdot\left[K_r\cdot(ss_1s_2+cc_1)+K_t\cdot c+K_a\cdot sc_2\right]$$

$$\alpha_{yx}=g(\phi_j)\cdot q\cdot(h_s)^{q-1}\cdot(-ss_1s_2)\cdot\left[K_r\cdot(-s_1s_2c+sc_1)+K_t\cdot s-K_a\cdot cc_2\right]$$

$$\alpha_{yy}=g(\phi_j)\cdot q\cdot(h_s)^{q-1}\cdot(cs_1s_2)\cdot\left[K_r\cdot(-s_1s_2c+sc_1)+K_t\cdot s-K_a\cdot cc_2\right]$$

$$\alpha_{yz}=g(\phi_j)\cdot q\cdot(h_s)^{q-1}\cdot(-s_1c_2)\cdot\left[K_r\cdot(-s_1s_2c+sc_1)+K_t\cdot s-K_a\cdot cc_2\right]$$

$$\alpha_{zx}=g(\phi_j)\cdot q\cdot(h_s)^{q-1}\cdot(-ss_1s_2)\cdot\left[K_r\cdot(-s_1c_2)+K_a\cdot s_2\right]$$

$$\alpha_{zy} = g\left(\phi_j\right)\cdot q\cdot\left(h_{\mathrm{s}}\right)^{q-1}\cdot\left(cs_1s_2\right)\cdot\left[K_{\mathrm{r}}\cdot\left(-s_1c_2\right)+K_{\mathrm{a}}\cdot s_2\right]$$

$$\alpha_{zz} = g\left(\phi_j\right)\cdot q\cdot\left(h_{\mathrm{s}}\right)^{q-1}\cdot\left(-s_1c_2\right)\cdot\left[K_{\mathrm{r}}\cdot\left(-s_1c_2\right)+K_{\mathrm{a}}\cdot s_2\right]$$

Where g($\phi_j$) represents the cutting state[7]. The cutter tooth is involved in cutting when its value is one. Otherwise, the teeth will not cut the workpiece; $q$ is the exponent constant; $h_s$ denotes the static chip thickness[6]; The parameters ($K_{\mathrm{r}}$, $K_{\mathrm{t}}$, and $K_{\mathrm{a}}$) are the milling force coefficients; $s$=sin ($\phi_j$), $c$=cos ($\phi_j$), $s_1$=sin ($\alpha$), $c_1$=cos ($\alpha$), $s_2$=sin ($\gamma$) and $c_2$=cos ($\gamma$).Based on the above analysis, the vibration energy of single system is obtained by Eq. (25).

In stage two, *R/C* vibration is bound to accelerate energy accumulation in *C/R*. As the depth of cut continues to increase, both the RMS and CMS are unstable. Thus, the critical curve ($R_cC_c$) between stage two and stage three should be determined. It may assume that the dynamic displacements along three coordinate directions are $Q_{C/R,x}$, $Q_{C/R,y}$ and $Q_{C/R,z}$ when the *C/R* starts to vibrate. The dynamic milling force could be displayed as:

$$\begin{bmatrix} dF_{C/R,X}\left(a,b\right) \\ dF_{C/R,Y}\left(a,b\right) \\ dF_{C/R,Z}\left(a,b\right) \end{bmatrix} = \Psi\cdot\chi\left(j\right)\cdot\begin{bmatrix} Q_{C/R,X}\left(a,b\right) \\ Q_{C/R,Y}\left(a,b\right) \\ Q_{C/R,Z}\left(a,b\right) \end{bmatrix} \tag{S31}$$

The dynamic milling force of *R/C* system can be expressed as:

$$\begin{bmatrix} dF_{R/C,X}\left(a,b\right) \\ dF_{R/C,Y}\left(a,b\right) \\ dF_{R/C,Z}\left(a,b\right) \end{bmatrix} = \Psi\cdot\chi\left(j\right)\cdot\begin{bmatrix} Q_{R/C,X}\left(a,b\right) \\ Q_{R/C,Y}\left(a,b\right) \\ Q_{R/C,Z}\left(a,b\right) \end{bmatrix} \tag{S32}$$

$$\begin{bmatrix} Q_{R/C,X}\left(a,b\right) \\ Q_{R/C,Y}\left(a,b\right) \\ Q_{R/C,Z}\left(a,b\right) \end{bmatrix} = \begin{bmatrix} \dfrac{dF_{R/C,X}\left(a,b,k\right)}{K_{R/C,X}\left(a,b,k\right)} \\ \dfrac{dF_{R/C,Y}\left(a,b,k\right)}{K_{R/C,Y}\left(a,b,k\right)} \\ \dfrac{dF_{R/C,Z}\left(a,b,k\right)}{K_{R/C,Z}\left(a,b,k\right)} \end{bmatrix} \tag{S33}$$

Meantime, the $dF_{C/R}$ and $dF_{R/c}$ are the relationship of acting force and reaction force as:

$$\begin{bmatrix} dF_{C/R,x}\left(a,b\right) \\ dF_{C/R,y}\left(a,b\right) \\ dF_{C/R,z}\left(a,b\right) \end{bmatrix} = -\begin{bmatrix} dF_{R/C,x}\left(a,b\right) \\ dF_{R/C,y}\left(a,b\right) \\ dF_{R/C,z}\left(a,b\right) \end{bmatrix} \tag{S34}$$

Substituting the Eq. (S32), Eq. (S33) and Eq. (S34) into Eq. (S31), the $dF_{C/R}$ can be written as:

$$\begin{bmatrix} dF_{C/R,X}\left(a,b,k\right) \\ dF_{C/R,Y}\left(a,b,k\right) \\ dF_{C/R,Z}\left(a,b,k\right) \end{bmatrix} = -\Psi^2 \cdot \chi^2\left(j\right) \cdot J \cdot \begin{bmatrix} Q_{C/R,X}\left(a,b,k\right) \\ Q_{C/R,Y}\left(a,b,k\right) \\ Q_{C/R,Z}\left(a,b,k\right) \end{bmatrix} \tag{S35}$$

$$J = \begin{bmatrix} \dfrac{1}{K_{R/C,X}\left(a,b,k\right)} & & \\ & \dfrac{1}{K_{R/C,Y}\left(a,b,k\right)} & \\ & & \dfrac{1}{K_{R/C,Z}\left(a,b,k\right)} \end{bmatrix} \tag{S36}$$

Among them, the $K_{R/C,X}$, $K_{R/C,Y}$ and $K_{R/C,Z}$ are the process stiffness of $R/C$ system in the three coordinate directions. They could be obtained by the Eq. (S26) and (S29). Finally, the second order FDM[4] servers as the analysis method of curve $R_cW_c$ based on the Eq. (S13) and (S35). Finally, the $R_cW_c$ is shown in Supplementary Fig. S3.

### 2.3 Stage three: Both RMS and CMS are unstable

The RMS and CMS are both instability when the cutting depth is above critical curve $R_cW_c$. Then, the self-excited vibration energy begins to accumulate quickly as shown in Supplementary Fig. S4. During RUMC-LT, the $dF_{RMS}(t)$ and $dF_{CMS}(t)$ are with the same magnitude but in opposite directions. According to the Eq. (S14), its dynamic expressions can be further written as:

$$\ddot{\Gamma}_{RMS}\left(t\right) + 2\left(\zeta_{RMS} + \zeta_p\right)\omega_{RMS}\dot{\Gamma}_{RMS}\left(t\right) + \omega_{RMS}^2\Gamma_{RMS}\left(t\right) = U_{RMS}^T dF_{RMS}\left(t\right) \tag{S37}$$

$$\ddot{\Gamma}_{CMS}\left(t\right) + 2\left(\zeta_{CMS} + \zeta_p\right)\omega_{CMS}\dot{\Gamma}_{CMS}\left(t\right) + \omega_{CMS}^2\Gamma_{CMS}\left(t\right) = -U_{CMS}^T dF_{CMS}\left(t\right) \tag{S38}$$

And the mass normalized mode shape for RMS ($U_{RMS}$) and CMS ($U_{CMS}$) can be displayed as:

$$U_{RMS} = \begin{bmatrix} u_{1,\mathrm{RMS}} & u_{2,\mathrm{RMS}} & \cdots & u_{m,\mathrm{RMS}} \end{bmatrix} \tag{S39}$$

$$U_{CMS} = \begin{bmatrix} u_{1,CMS} & u_{2,CMS} & \cdots & u_{n,CMS} \end{bmatrix} \tag{S40}$$

$$u_{\mathrm{m,RMS}} = \begin{bmatrix} u_{\mathrm{X},m,\mathrm{RMS}} & u_{Y,m,\mathrm{RMS}} & u_{Z,m,\mathrm{RMS}} \end{bmatrix}^T \tag{S41}$$

$$u_{n,CMS} = \begin{bmatrix} u_{\mathrm{X,n},CMS} & u_{Y,n,CMS} & u_{Z,n,CMS} \end{bmatrix}^T \tag{S42}$$

Meanwhile, the angular frequency and modal damping ratio are written as the follow matrixes:

$$\omega_{RMS} = \mathrm{diag}\left(\omega_{1,\mathrm{RMS}} \quad \omega_{2,\mathrm{RMS}} \quad \cdots \quad \omega_{m,\mathrm{RMS}}\right)_{m\cdot m} \tag{S43}$$

$$\omega_{CMS}=\mathrm{diag}\begin{pmatrix}\omega_{1,CMS} & \omega_{2,CMS} & \cdots & \omega_{m,CMS}\end{pmatrix}_{n\cdot n} \tag{S44}$$

$$\zeta_{RMS}=\mathrm{diag}\begin{pmatrix}\zeta_{1,\mathrm{RMS}} & \zeta_{2,\mathrm{RMS}} & \cdots & \zeta_{m,\mathrm{RMS}}\end{pmatrix}_{m\cdot m} \tag{S45}$$

$$\zeta_{CMS}=\mathrm{diag}\begin{pmatrix}\zeta_{1,CMS} & \zeta_{2,CMS} & \cdots & \zeta_{m,CMS}\end{pmatrix}_{m\cdot m} \tag{S46}$$

Finally, the coupling dynamic expression of RMS and CMS can be expressed as:

$$\ddot{\Gamma}_{RC}\left(t\right)+\left(2\zeta_{RC}\omega_{RC}\right)\dot{\Gamma}_{RC}\left(t\right)+\omega_{RC}\Gamma_{RC}\left(t\right)=U_{RC}^{T}dF_{RC}\left(t\right) \tag{S47}$$

Among them,

$$\Gamma_{RC}\left(t\right)=\begin{bmatrix}\Gamma_{RMS}\left(t\right)\\ \Gamma_{CMS}\left(t\right)\end{bmatrix}$$

$$\zeta_{RC}=\begin{bmatrix}\zeta_{RMS}+\zeta_{p} & \\ & \zeta_{CMS}+\zeta_{p}\end{bmatrix}$$

$$\omega_{RC}=\begin{bmatrix}\omega_{RMS} & \\ & \omega_{CMS}\end{bmatrix}$$

$$U_{RC}=\begin{bmatrix}U_{RMS} & -U_{CMS}\end{bmatrix}$$

Based on above analysis, the dynamic displacement $Q_f$ ($f$=RMS, CMS) can be calculated by the follow equation:

$$\begin{aligned}Q_{f,u}\left(a,b,k\right)&=\frac{dF_{f,u}\left(a,b,k\text{-}1\right)}{K_{f,k}}\\&=E+e^{-\frac{\xi_{f,u}\omega_{f,u}}{p_{f,u}(a,b)}}\left[\alpha_f\cdot\sin\left(\frac{\bar{\omega}_{f,u}}{p_{f,u}\left(a,b\right)}\right)+\beta_f\cdot\cos\left(\frac{\bar{\omega}_{f,u}}{p_{f,u}\left(a,b\right)}\right)\right]\end{aligned} \tag{S48}$$

$$\begin{aligned}E=&\frac{1}{\bar{\omega}_{f,u}}\int_0^{\frac{1}{p_{f,u}(a,b)}}dF_{f,u}\left(a,b,k-1,\tau\right)\cdot e^{-\omega_{f,u}\xi_{f,u}\left(\frac{1}{p_{f,u}(a,b)}-\tau\right)}\\&\cdot\sin\bar{\omega}_{f,u}\left(\frac{1}{p_{f,u}\left(a,b\right)}-\tau\right)d\tau\end{aligned}$$

Where $\alpha_f$ and $\beta_f$ are the Duhamel integral constant. They could be calculated by the Rayleigh damping theory[3]. The $K_{f,k}$ is the processing stiffness of $k$-th vibration which can be obtained by Eq. (S50).

For the multi-system chatter, its energy accumulation expression could be written as:

$$E_v^{RC}=2\pi^2\left(\sum_{u=1}^{m_e}m_{RMS,u}\,p_{RMS,u}^2Q_{RMS,u}^2+\sum_{u=1}^{n_e}m_{CMS,u}\,p_{CMS,u}^2Q_{CMS,u}^2\right) \tag{S49}$$

In Eq. (S49), the $Q_f(t)$ is related to the $dF_f(t)$. The coupling process of force and displacement could be further expressed as:

$$U_{f,u}^{T} dF_{f,u}\left(a,b,0\right)=\Psi\cdot\sum_{j=1}^{N_e}\chi\left(j\right)\cdot\left|Q_{RMS,u}\left(a,b,0\right)-Q_{CMS,u}\left(a,b,0\right)\right|$$

$$\begin{aligned}U_{f,u}^{T} dF_{f,u}\left(a,b,1\right)&=\Psi\cdot\sum_{j=1}^{N_e}\chi\left(j\right)\cdot\left[\frac{dF_{RMS,u}\left(a,b,0\right)}{K_{RMS,1}}-\frac{dF_{CMS,u}\left(a,b,0\right)}{K_{CMS,1}}\right]\\&=\Psi\cdot\sum_{j=1}^{N_e}\chi\left(j\right)^2\cdot\left(\frac{1}{K_{RMS,1}}-\frac{1}{K_{CMS,1}}\right)\cdot\left|Q_{RMS,u}\left(a,b,0\right)-Q_{CMS,u}\left(a,b,0\right)\right|\end{aligned}$$

$$\begin{aligned}U_{f,u}^{T} dF_{f,u}\left(a,b,2\right)&=\Psi\cdot\sum_{j=1}^{N_e}\chi\left(j\right)\cdot\left[\frac{dF_{RMS,u}\left(a,b,1\right)}{K_{RMS,2}}-\frac{dF_{CMS,u}\left(a,b,1\right)}{K_{CMS,2}}\right]\\&=\Psi\cdot\sum_{j=1}^{N_e}\chi\left(j\right)^3\cdot\left[\frac{1}{K_{RMS,1}\cdot K_{RMS,2}}-\frac{1}{K_{CMS,1}\cdot K_{CMS,2}}\right]\cdot\left|Q_{RMS,u}\left(a,b,0\right)-Q_{CMS,u}\left(a,b,0\right)\right|\end{aligned}$$

$$\cdots\cdots$$

$$\begin{aligned}U_{f,u}^{T} dF_{f,u}\left(a,b,k\right)&=\Psi\cdot\sum_{j=1}^{N_e}\chi\left(j\right)\cdot\left[\frac{dF_{RMS,u}\left(a,b,k\text{-}1\right)}{K_{RMS,k}}-\frac{dF_{CMS,u}\left(a,b,k\text{-}1\right)}{K_{CMS,k}}\right]\\&=\Psi\cdot\sum_{j=1}^{N_e}\chi\left(j\right)^{k+1}\cdot\left[\frac{1}{K_{RMS,1}\cdot K_{RMS,2}\cdots K_{RMS,k}}-\frac{1}{K_{CMS,1}\cdot K_{CMS,2}\cdots K_{CMS,k}}\right]\\&\quad\cdot\left|Q_{RMS,u}\left(a,b,0\right)+Q_{CMS,u}\left(a,b,0\right)\right|\end{aligned}\tag{S50}$$

Among them, the $dF_{RMS}$ and $K_{RMS,\ k}$ are the dynamic milling force and processing stiffness of robots. The $dF_{CMS}$ and $K_{CMS,\ k}$ are the dynamic milling force and processing stiffness of component. According to the value convergence of vibration energy field, the vibration amplitude can be calculated when RUMC-LT system keeps in stable vibration state. At this time, the value of dynamic milling forces is closed to constant. Finally, the chatter stability calculation result is shown in Supplementary Excel 1.

# Supplementary Results

## Robotic milling experiment platform

As presented in Supplementary Fig. S5, the RUMC-LT experiments are carried out to verify the stability boundary curves (Fig. 5a). The height of hollow cylindrical component with low stiffness has 530mm and the machined surface diameter is 300mm. Its material is aluminum alloy (Al7075-T7) and the stiffness value is 1.08×10^6 N/m. The type of industrial robots is KUKA KR500 R2830 MT/FLR. The rotary ultrasonic machining device is designed by the project team. includes an ultrasonic generator, an ultrasonic tool shank and a milling cutter. The ultrasonic generator transmits electric signal firstly. Then, the transducer in ultrasonic tool shank could transform it to high frequency vibration. Furthermore, this mechanical vibration signal is amplified when it is transported to the LT amplitude transformer. Finally, under the effect of the oblique grooves, a LT composite vibration phenomenon appears on the end of the milling cutter.

In this paper, the robotic modal parameters are obtained by standard modal hampering experiments. Robotic milling plates experiments are applied for determining the milling force coefficients as shown in Supplementary Table S4. In addition, the acceleration measurement module and the displacement measurement module are used to record the acceleration and displacement signals during the machining process.

As shown in Supplementary Fig. S6, the type of industrial robot is KUKA KR210-R2700 EXTRA. The size of rigid plate (Al7075-T7) is 150mm×80mm×5mm. The CFRP laminate is a two-way interwoven layered structure, the laying direction is 0° and 90°, and the base material is T300 epoxy resin. The workpiece size is 200mm×150mm×2mm. Meanwhile, the robotic pose and modal parameters are shown in Supplementary Table. S5 and Supplementary Table. S6.

**Robotic milling experiment results**

In this paper, the stability boundary curves and the relationship model accuracy should be verified by the experimental results. The Point 1-Point 25 of Fig. 5a are selected for milling parameters. The milling signals of Point 1-Point 20 are presented in Supplementary Fig. S7 to Supplementary Fig. S26 while the Point 21-Point 25 are illustrated in Fig. 5b. Finally, the experimental results are in good agreement with the theoretical calculation results.

In addition, the calculation principle of relationship model accuracy is shown in Main Text. The 100 groups experimental data is presented in Supplementary Excel 2.

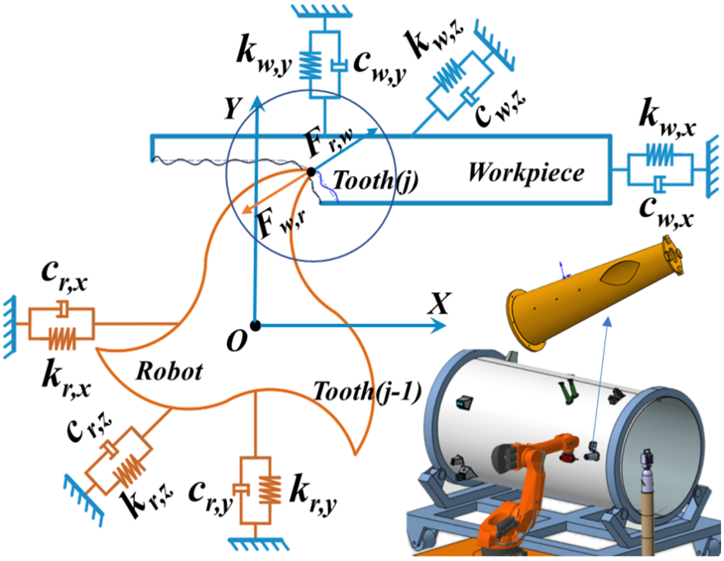


**Supplementary Fig. S1. RUMC-LT dynamic.** Among them, $c_{r,x}$, $c_{r,y}$ and $c_{r,z}$ are the RMS damping; $k_{r,x}$, $k_{r,y}$, $k_{r,z}$ are the RMS stiffness; $c_{w,x}$, $c_{w,y}$ and $c_{w,z}$ are the CMS damping; $k_{w,x}$, $k_{w,y}$, $k_{w,z}$ are the CMS stiffness; $F_{w,r}$ and $F_{r,w}$ are the interaction forces between RMS and CMS. The robotic type is KUKA KR500 R2830 MT/FLR. The component is the height of hollow cylindrical component with low stiffness, which has 530mm and the machined surface diameter is 300mm. Its material is aluminum alloy (Al7075-T7).

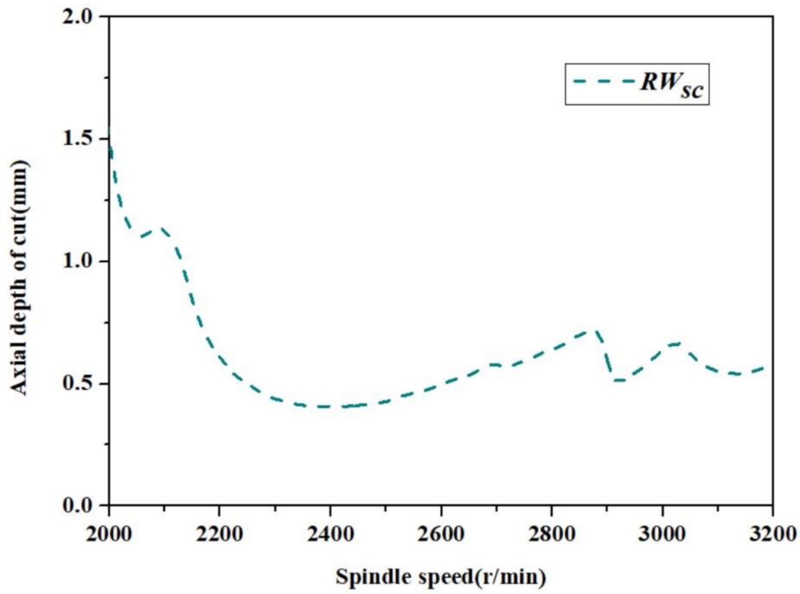


**Supplementary Fig. S2. Stability analysis results in stage one.** Under the curve $RW_{sc}$, the machining parameters are stable. Otherwise, they are unstable. milling parameters: down milling, feed in *X* direction and feed rate is 60mm/min, 50% radial immersion of cutter. Ultrasonic vibration frequency is 30000Hz. The longitudinal and torsional amplitudes are the 8.0μm and 5.3μm, respectively.

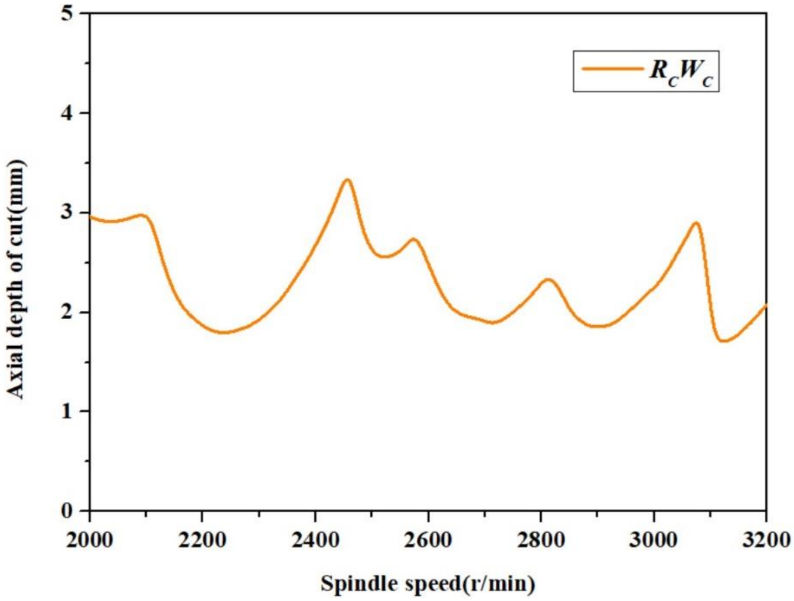


**Supplementary Fig. S3. Stability analysis results in stage two.** Above the curve $R_cW_c$, both the RMS and CMS are unstable. Milling parameters: down milling, feed in $X$ direction and feed rate is 60mm/min, 50% radial immersion of cutter. Ultrasonic vibration frequency is 30000Hz. The longitudinal and torsional amplitudes are the 8.0μm and 5.3μm, respectively.

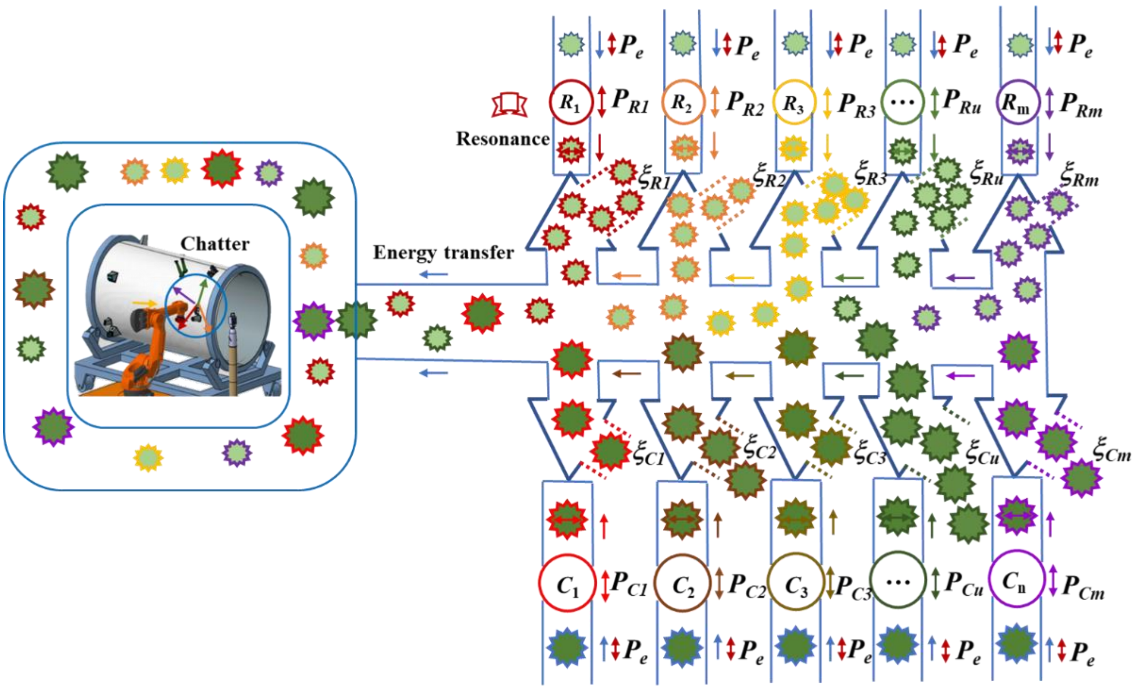


**Supplementary Fig. S4. Vibration energy fields coupling between low stiffness systems at same frequency and phase.** $C_1$ to $C_m$ are robotic modes and $P_{C1}$ to $P_{Cm}$ shows corresponding modal frequency. In addition, $\xi_{C1}$ to $\xi_{Cm}$ are component damping ratios. $R_1$ to $R_m$ are robotic modes and $P_{R1}$ to $P_{Rm}$ shows corresponding modal frequency. In addition, $\xi_{R1}$ to $\xi_{Rm}$ are robotic damping ratios.

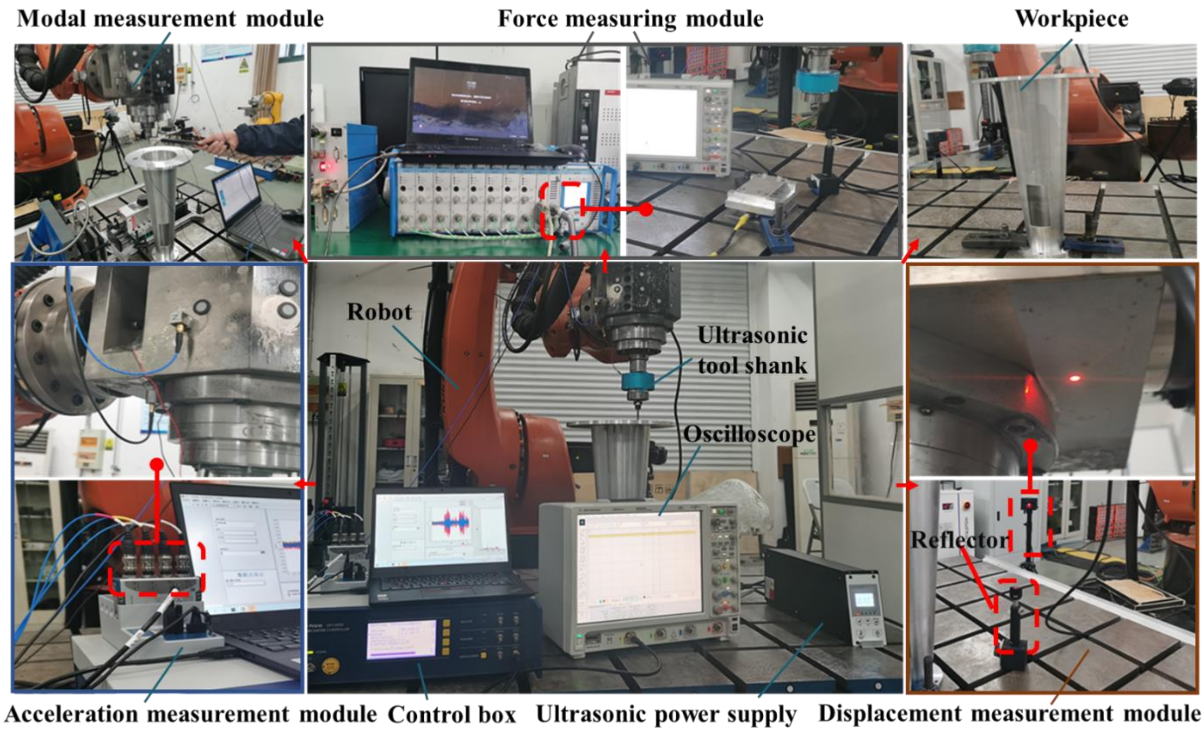


**Supplementary Fig. S5. RUMC-LT experimental site.**

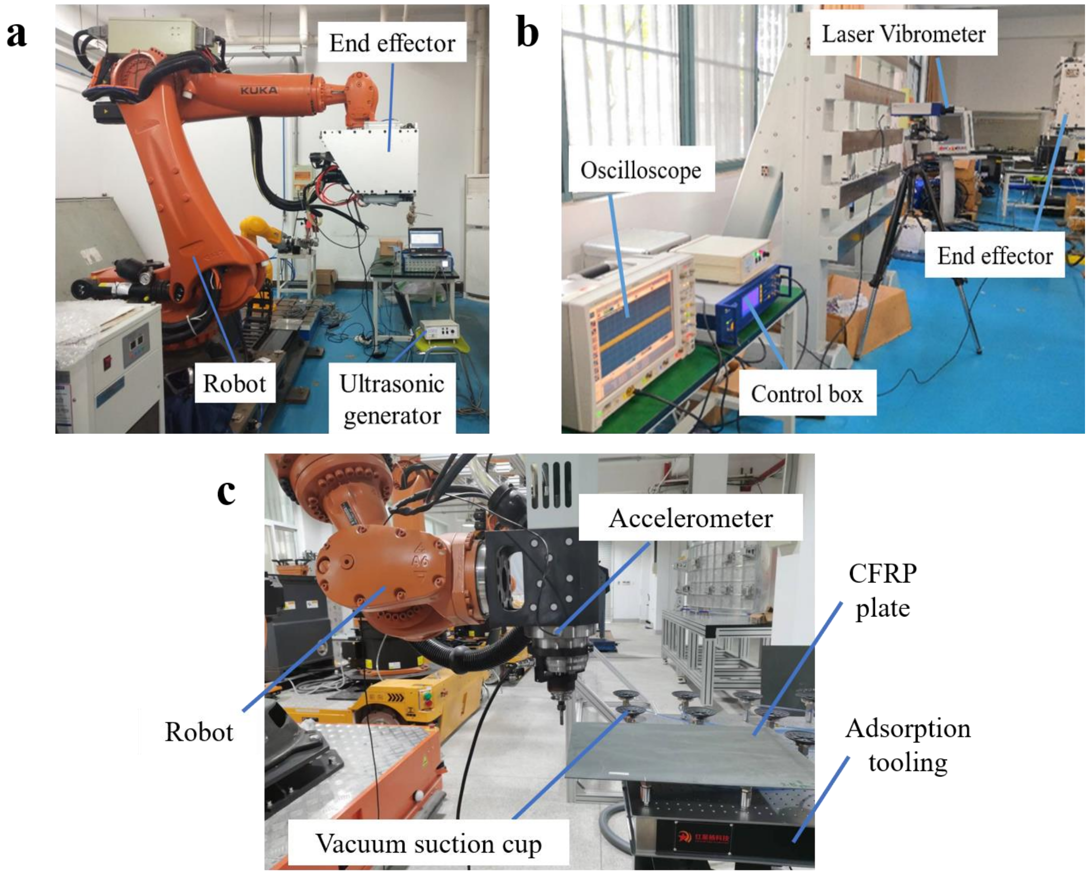


**Supplementary Fig. S6. Robotic milling aluminum alloy plate and CFRP plate. a** Industrial robot. **b** Amplitude measuring **c** Edge milling experiments of robot.

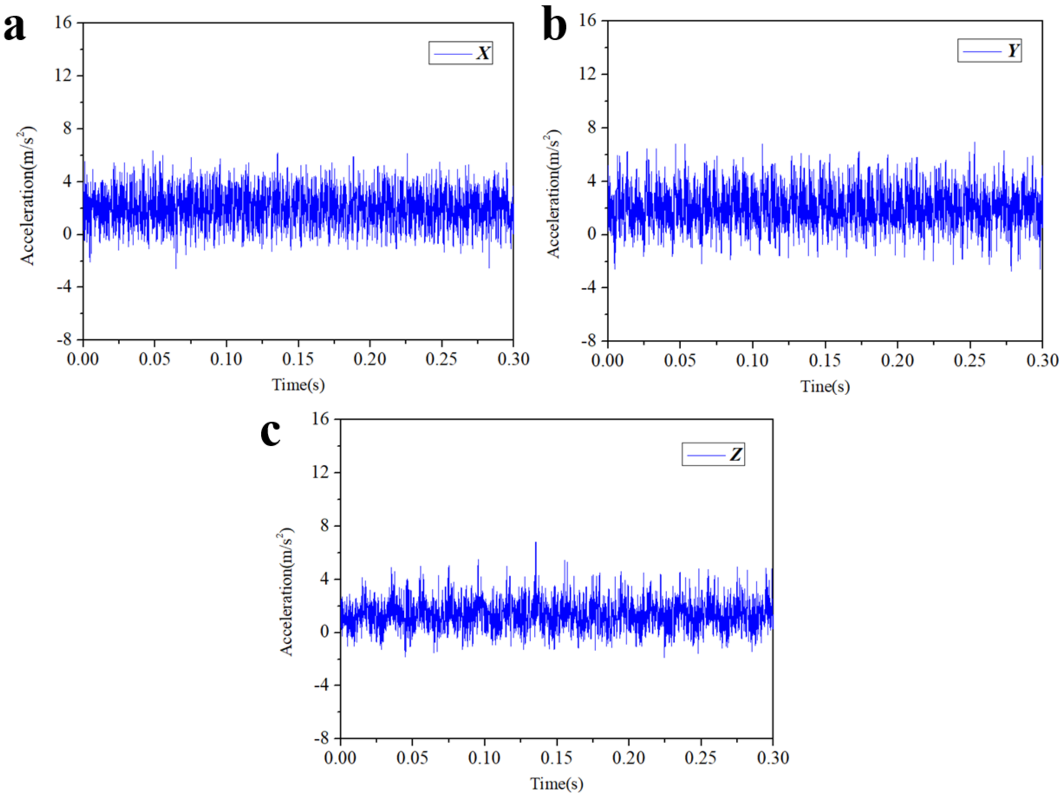


**Supplementary Fig. S7. RUMC-LT acceleration signals in point 1 of Fig. 5a. a** *X* represents feed direction. **b** *Y* means perpendicular to the feed direction. **c** *Z* is along the axial direction of milling tool.

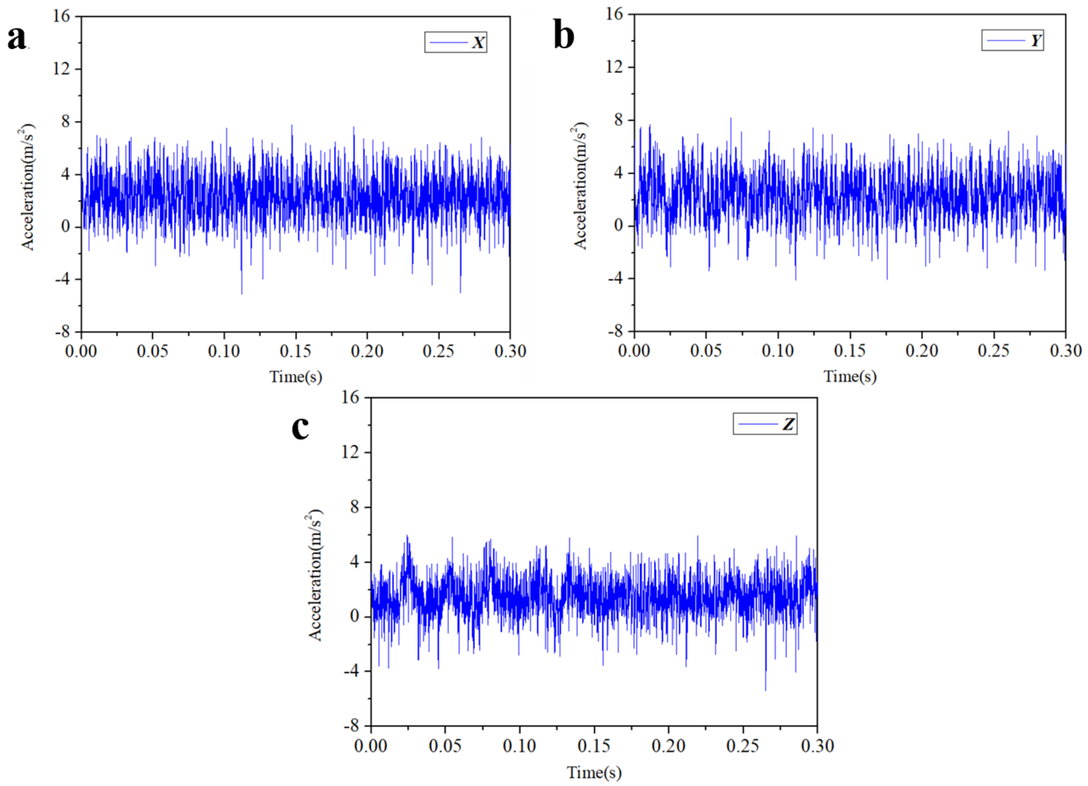


**Supplementary Fig. S8. RUMC-LT acceleration signals in point 2 of Fig. 5a. a** *X* represents feed direction. **b** *Y* means perpendicular to the feed direction. **c** *Z* is along the axial direction of milling tool.

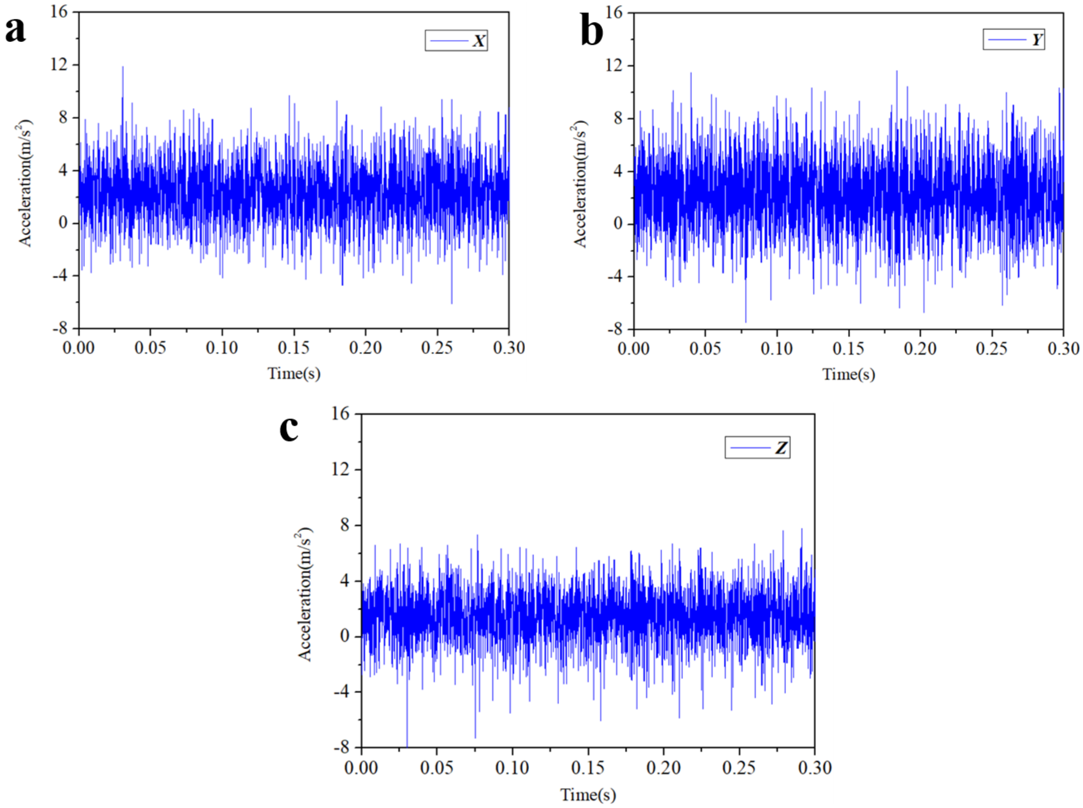


**Supplementary Fig. S9. RUMC-LT acceleration signals in point 3 of Fig. 5a. a** *X* represents feed direction. **b** *Y* means perpendicular to the feed direction. **c** *Z* is along the axial direction of milling tool.

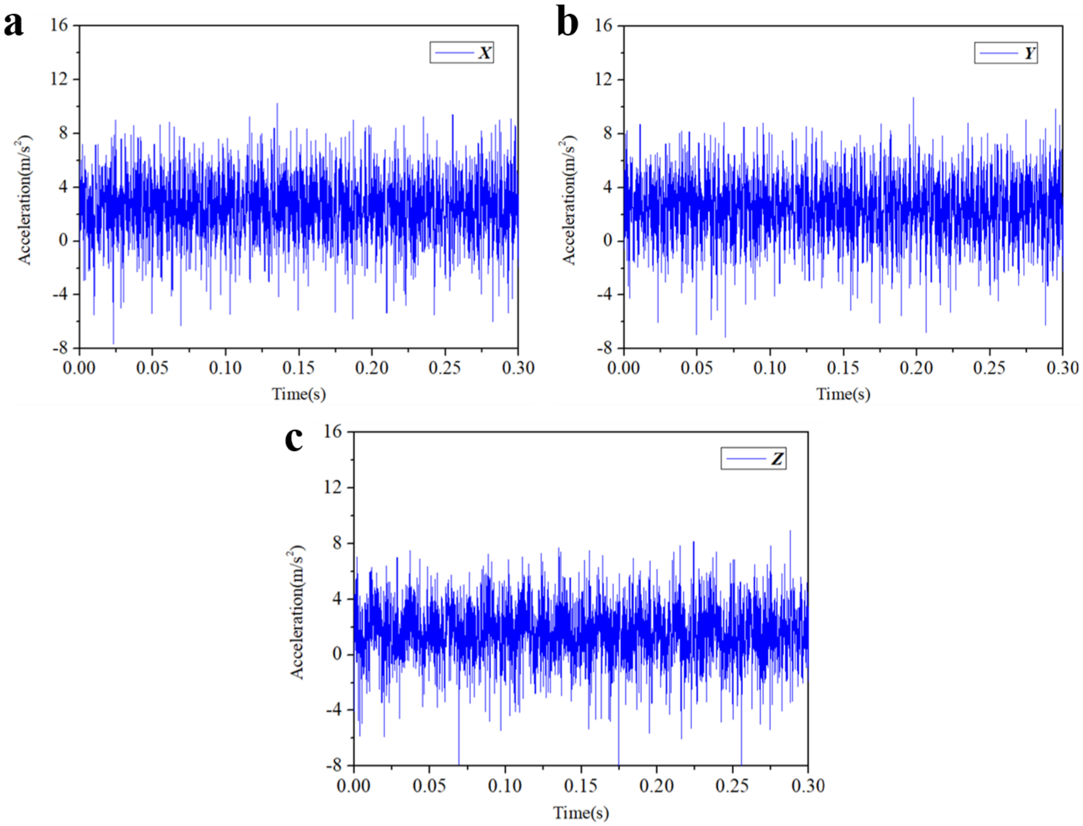


**Supplementary Fig. S10. RUMC-LT acceleration signals in point 4 of Fig. 5a. a** *X* represents feed direction. **b** *Y* means perpendicular to the feed direction. **c** *Z* is along the axial direction of milling tool.

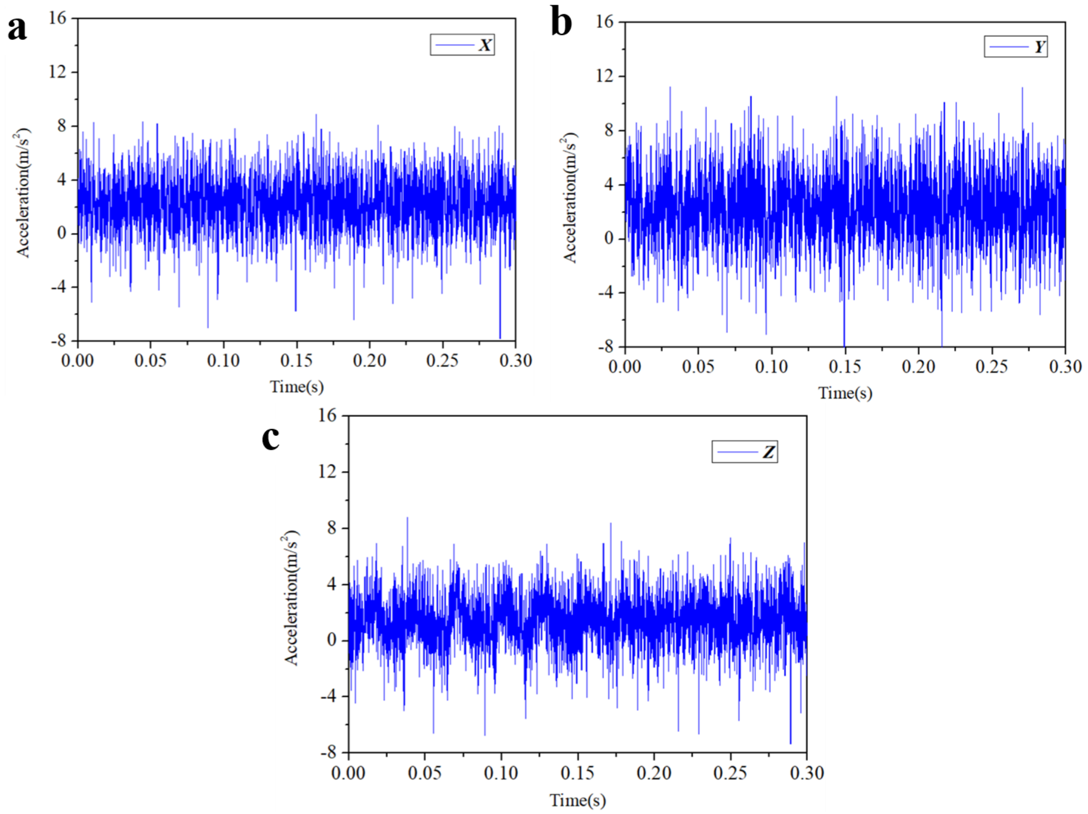


**Supplementary Fig. S11. RUMC-LT acceleration signals in point 5 of Fig. 5a. a** *X* represents feed direction. **b** *Y* means perpendicular to the feed direction. **c** *Z* is along the axial direction of milling tool.

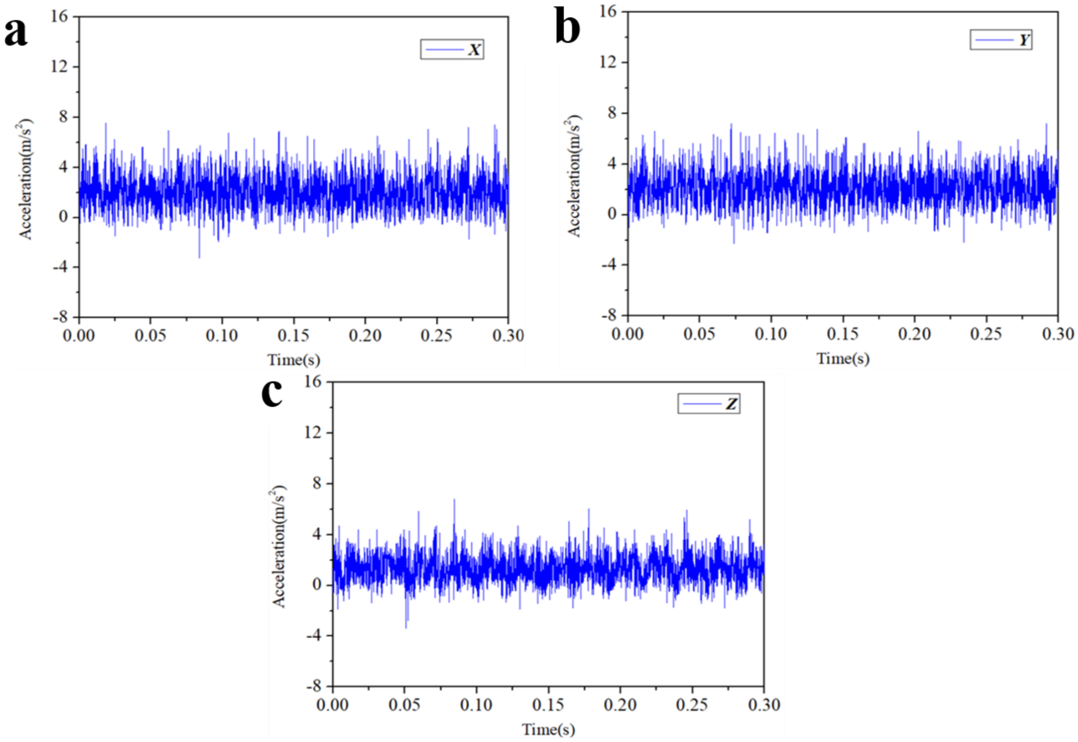


**Supplementary Fig. S12. RUMC-LT acceleration signals in point 6 of Fig. 5a. a** *X* represents feed direction. **b** *Y* means perpendicular to the feed direction. **c** *Z* is along the axial direction of milling tool.

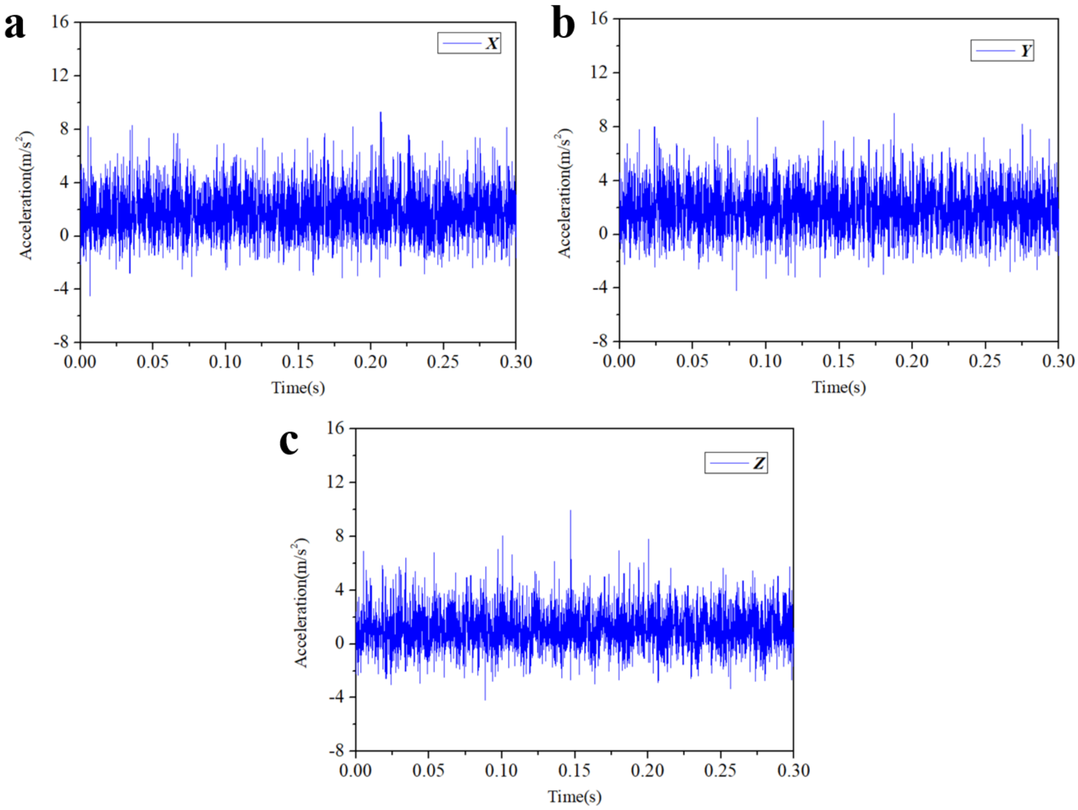


**Supplementary Fig. S13. RUMC-LT acceleration signals in point 7 of Fig. 5a. a** *X* represents the feed direction. **b** *Y* means perpendicular to the feed direction. **c** *Z* is along the axial direction of milling tool.

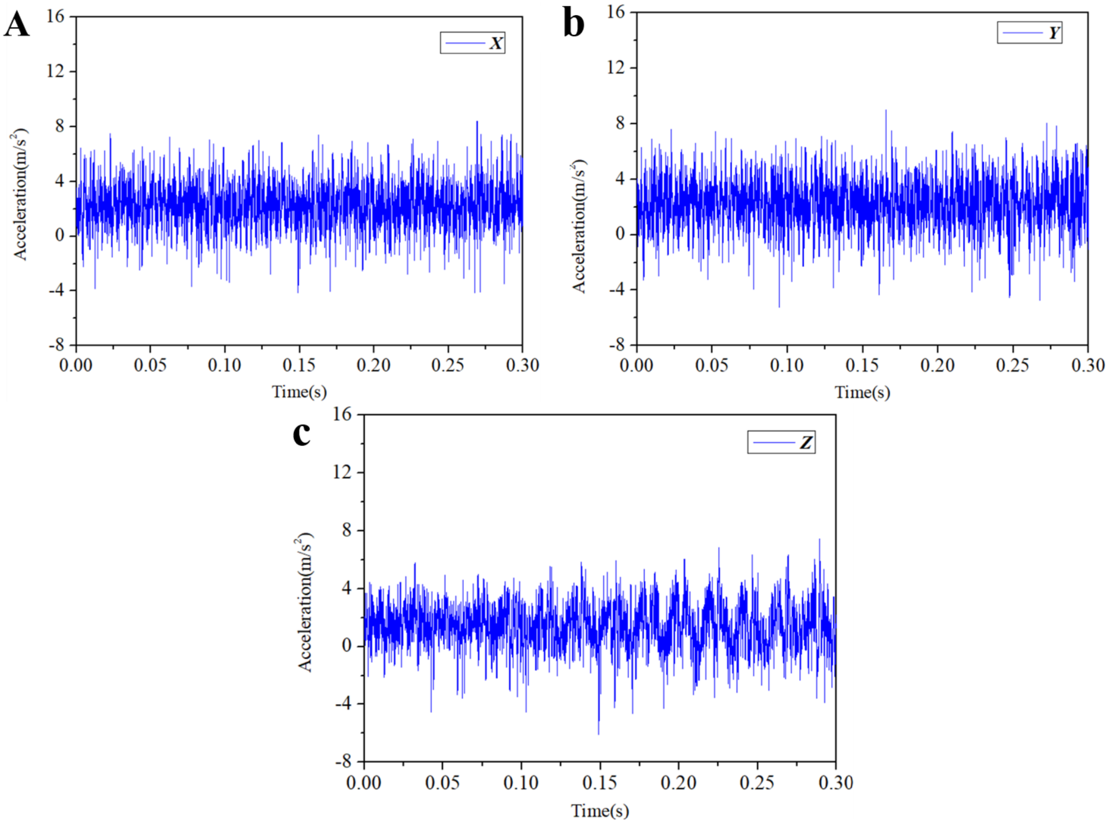


**Supplementary Fig. S14. RUMC-LT acceleration signals in point 8 of Fig. 5a. a** *X* represents feed direction. **b** *Y* means perpendicular to the feed direction. **c** *Z* is along the axial direction of milling tool.

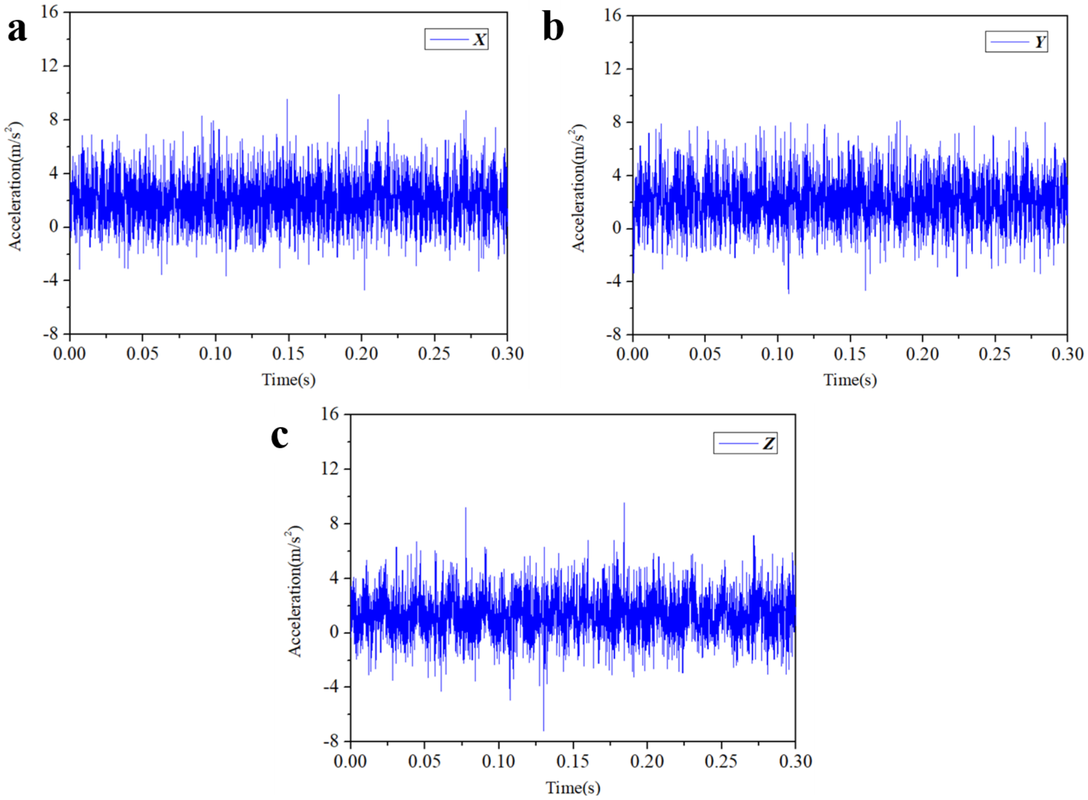


**Supplementary Fig. S15. RUMC-LT acceleration signals in point 9 of Fig. 5a. a** *X* represents feed direction. **b** *Y* means perpendicular to the feed direction. **c** *Z* is along the axial direction of milling tool.

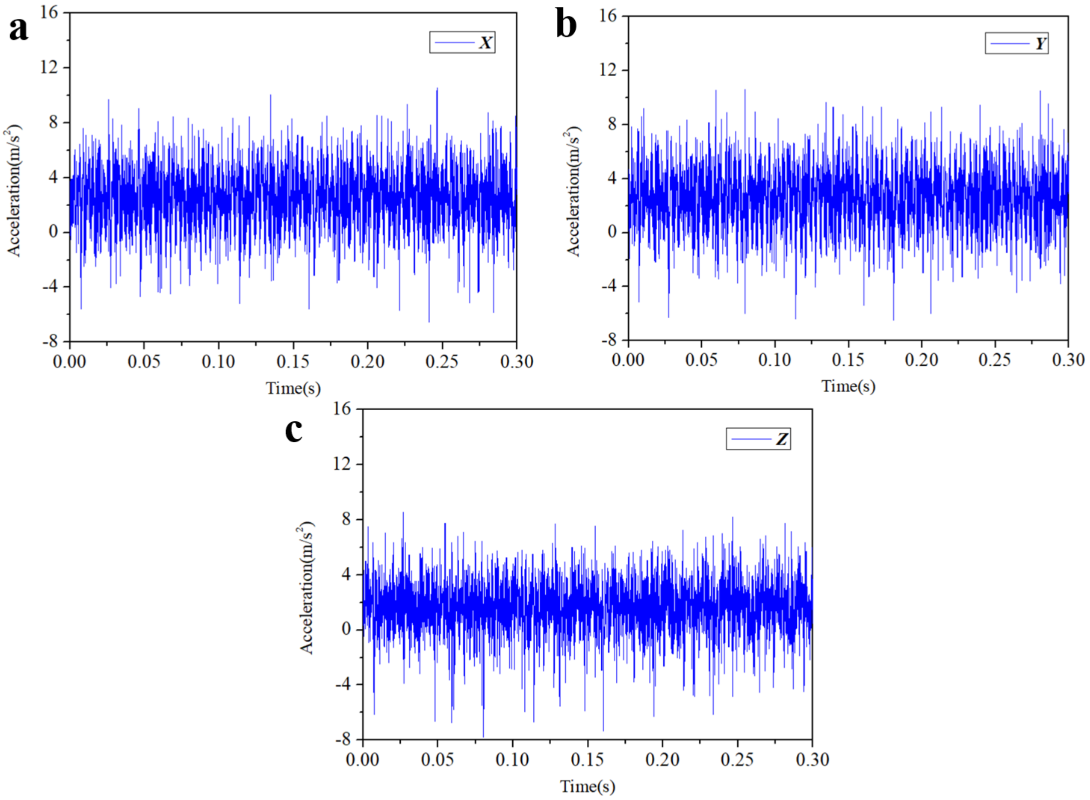


**Supplementary Fig. S16. RUMC-LT acceleration signals in point 10 of Fig. 5a. a** *X* represents feed direction. **b** *Y* means perpendicular to the feed direction. **C** *Z* is along the axial direction of milling tool.

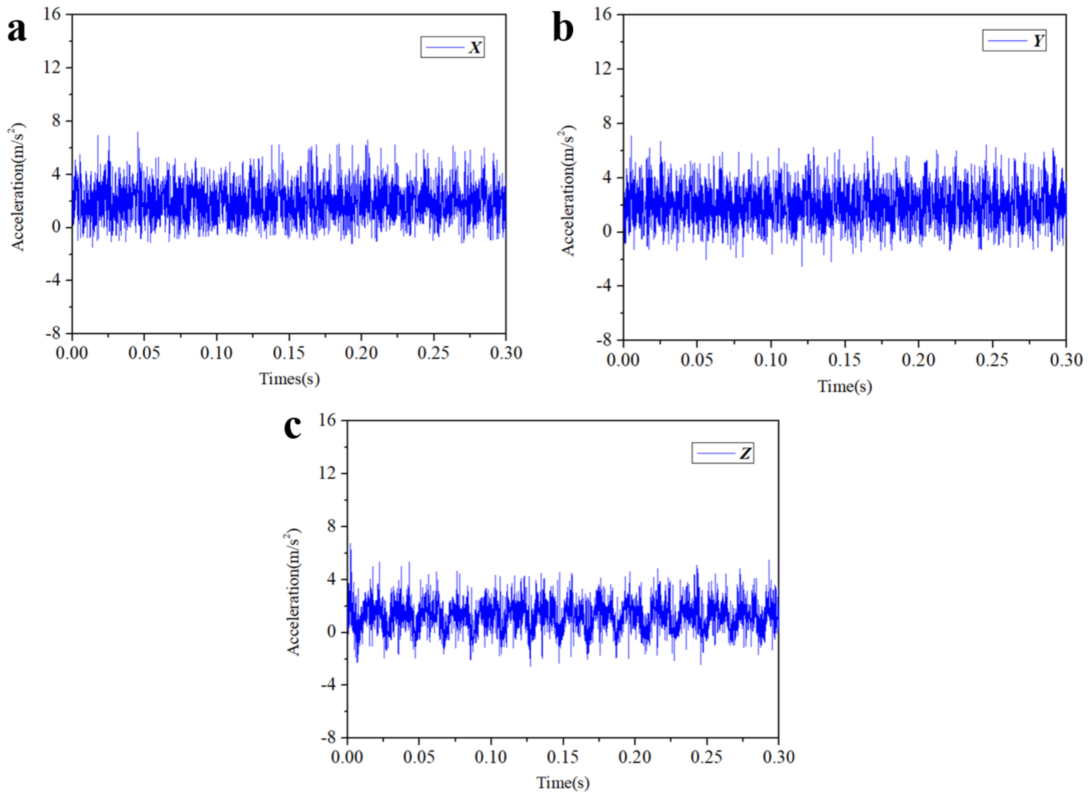


**Supplementary Fig. S17. RUMC-LT acceleration signals in point 11 of Fig. 5a. a** *X* represents feed direction. **b** *Y* means perpendicular to the feed direction. **c** *Z* is along the axial direction of milling tool.

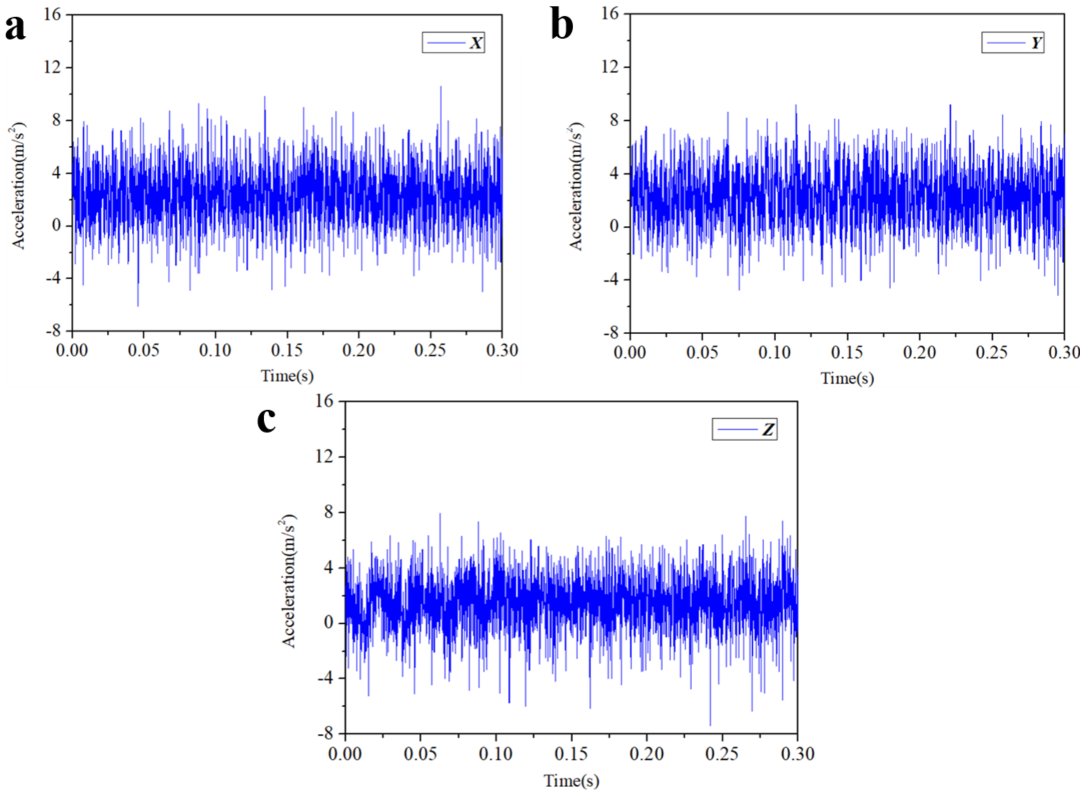


**Supplementary Fig. S18. RUMC-LT acceleration signals in point 12 of Fig. 5a. a** *X* represents feed direction. **b** *Y* means perpendicular to the feed direction. **c** *Z* is along the axial direction of milling tool.

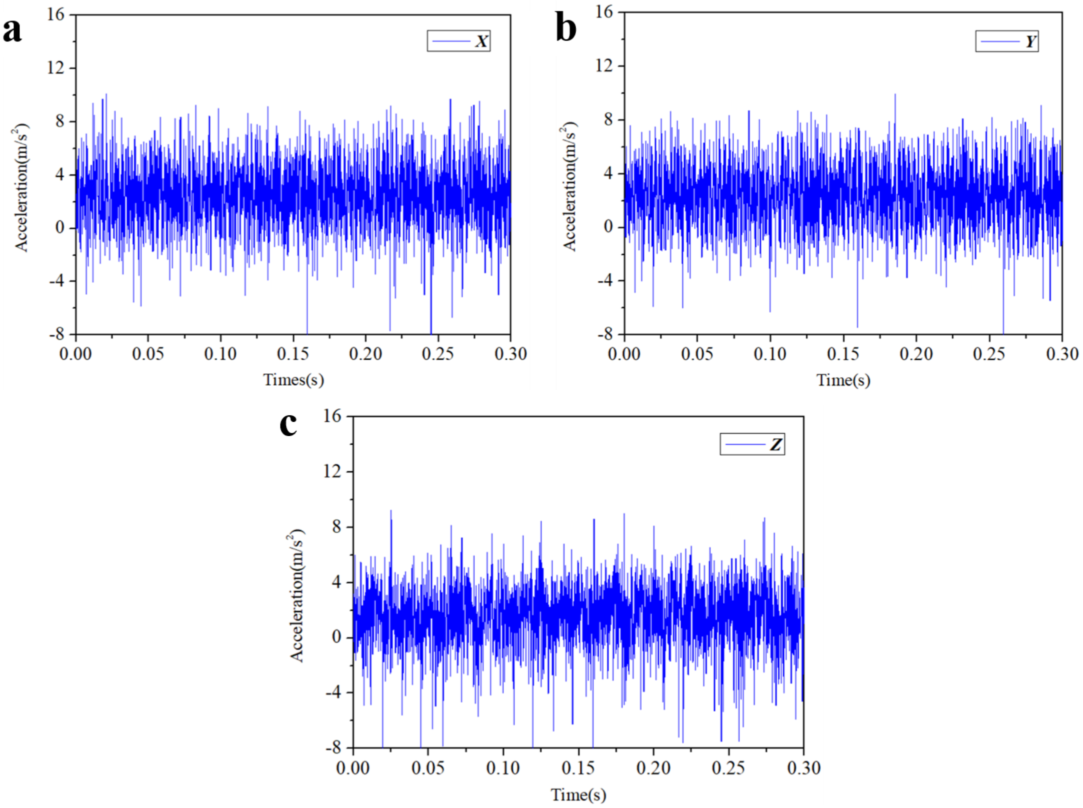


**Supplementary Fig. S19. RUMC-LT acceleration signals in point 13 of Fig. 5a. a** *X* represents feed direction. **b** *Y* means perpendicular to the feed direction. **c** *Z* is along the axial direction of milling tool.

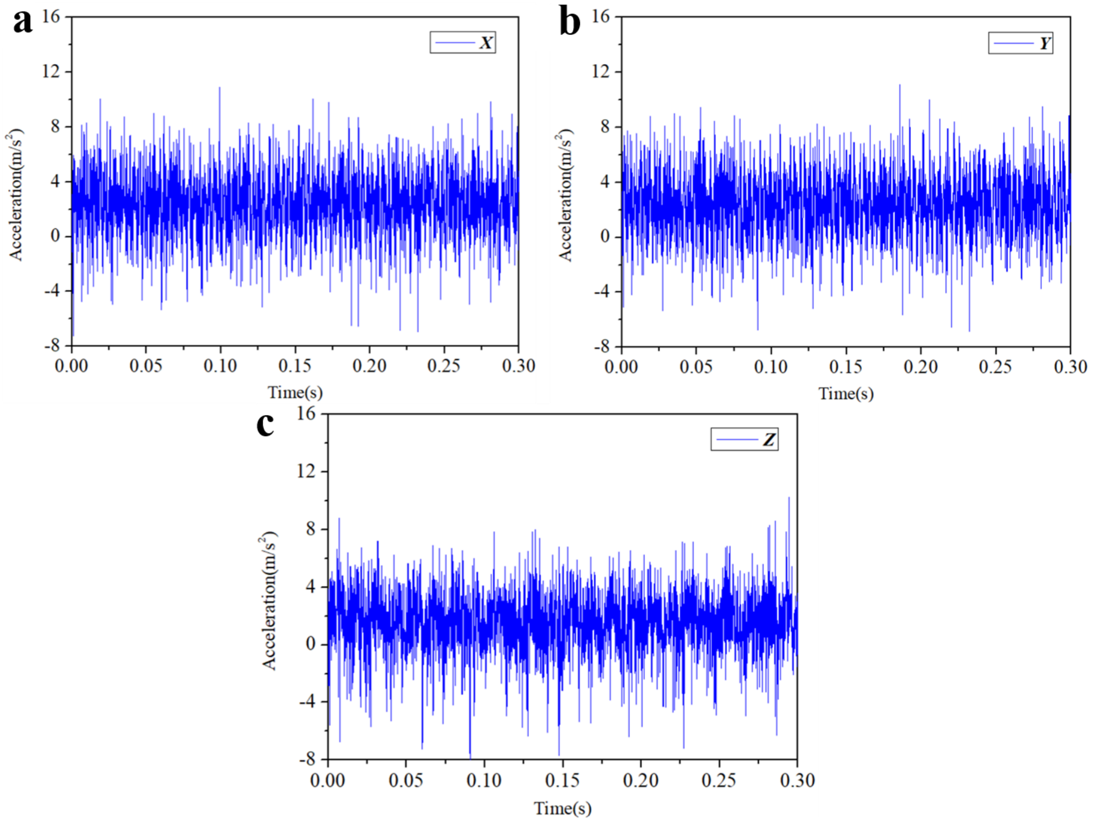


**Supplementary Fig. S20. RUMC-LT acceleration signals in point 14 of Fig. 5a. a** *X* represents feed direction. **b** *Y* means perpendicular to the feed direction. **c** *Z* is along the axial direction of milling tool.

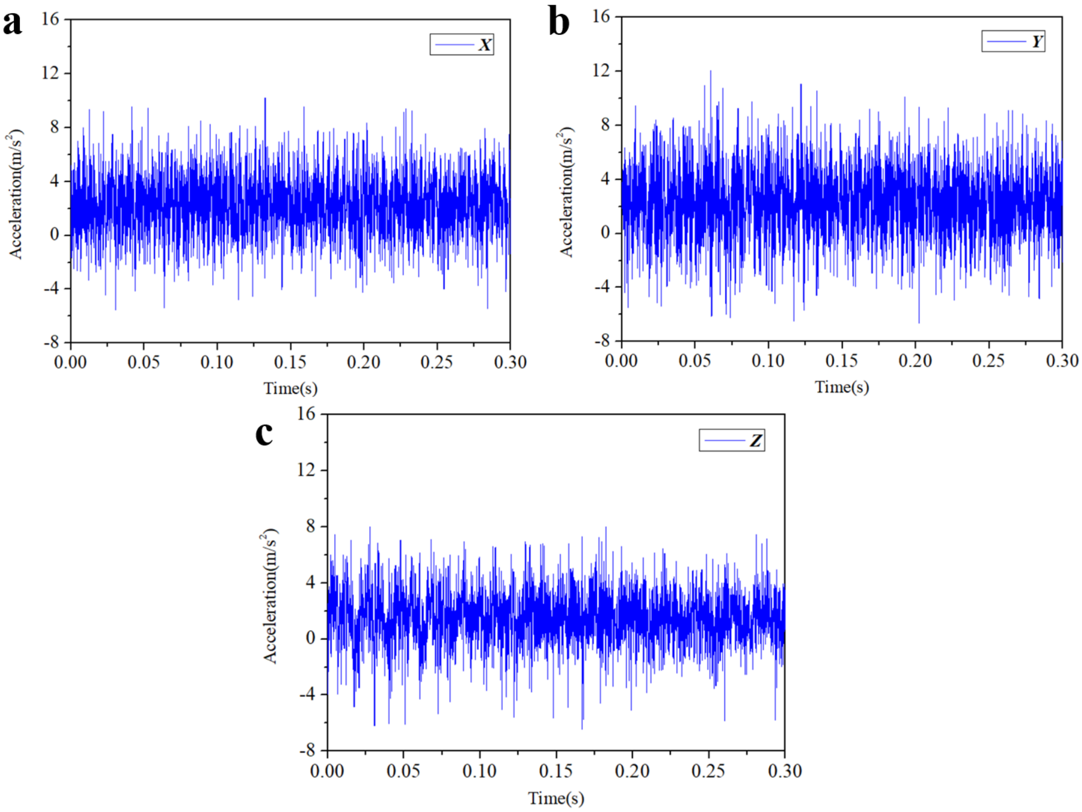


**Supplementary Fig. S21. RUMC-LT acceleration signals in point 15 of Fig. 5a. a** *X* represents feed direction. **b** *Y* means perpendicular to the feed direction. **c** *Z* is along the axial direction of milling tool.

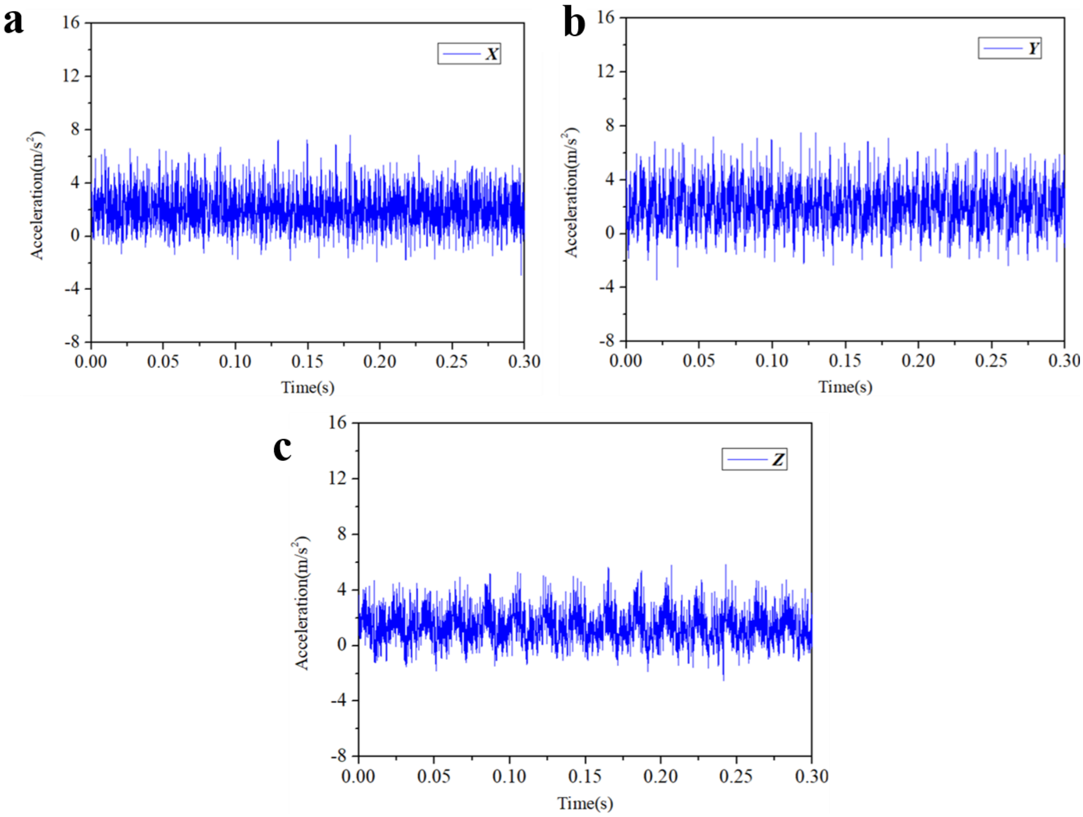


**Supplementary Fig. S22. RUMC-LT acceleration signals in point 16 of Fig. 5a. a** *X* represents feed direction. **b** *Y* means perpendicular to the feed direction. **c** *Z* is along the axial direction of milling tool.

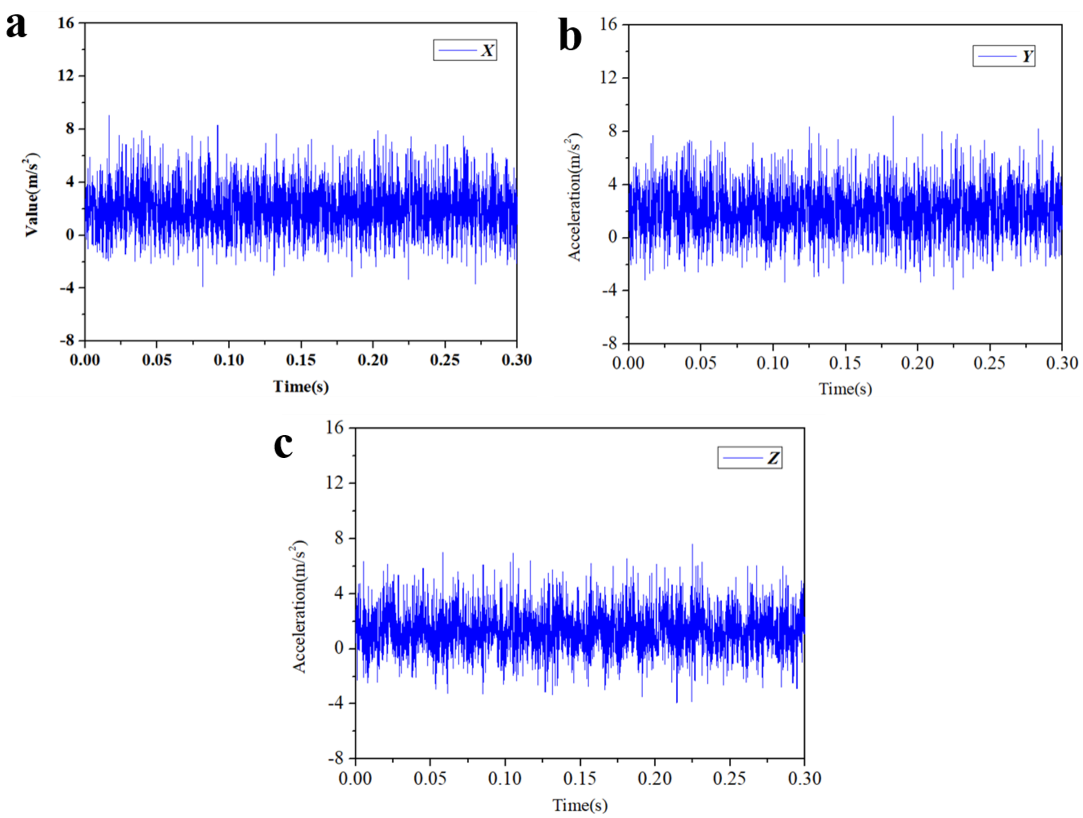


**Supplementary Fig. S23. RUMC-LT acceleration signals in point 17 of Fig. 5a. a** *X* represents feed direction. **b** *Y* means perpendicular to the feed direction. **c** *Z* is along the axial direction of milling tool.

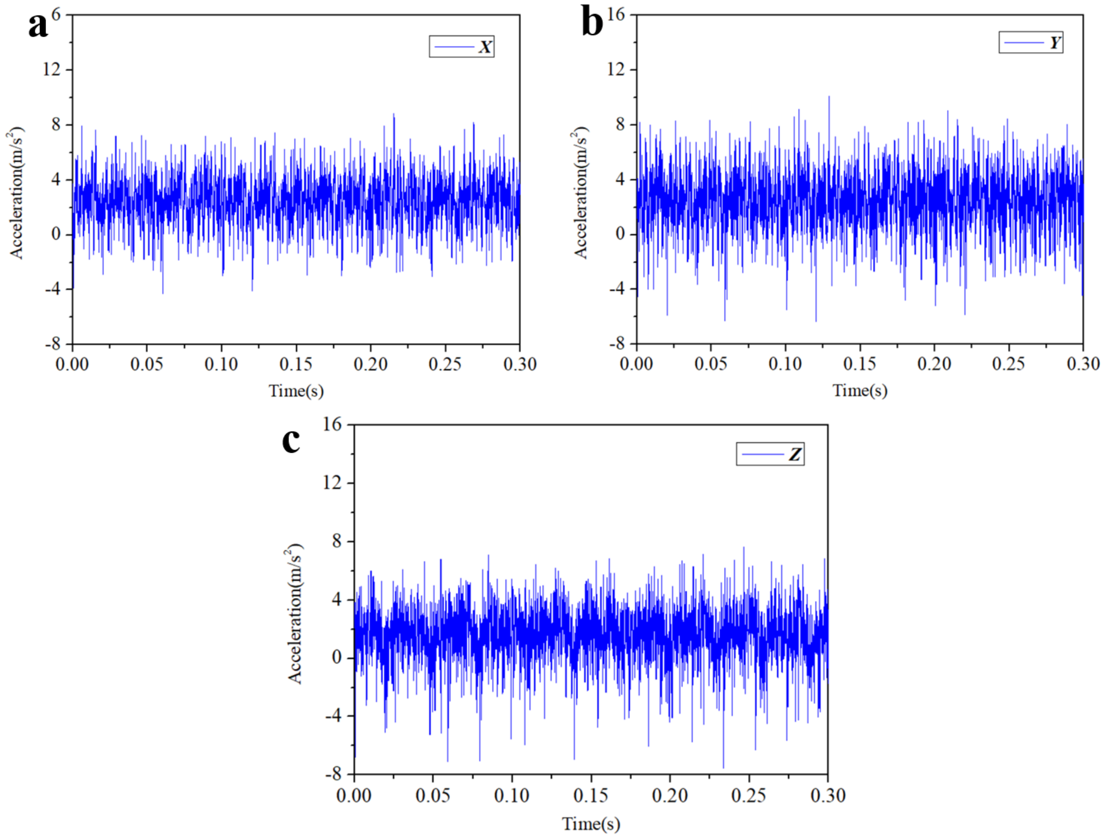


**Supplementary Fig. S24. RUMC-LT acceleration signals in point 18 of Fig. 5a. a** *X* represents feed direction. **b** *Y* means perpendicular to the feed direction. **c** *Z* is along the axial direction of milling tool.

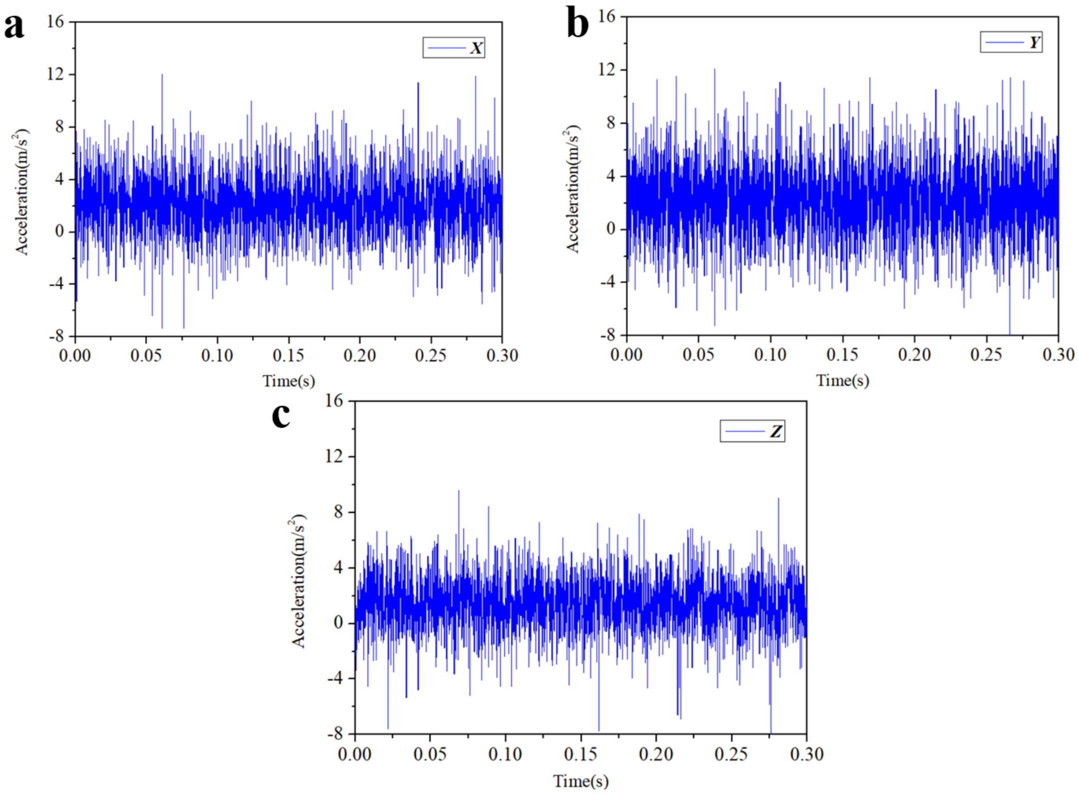


**Supplementary Fig. S25. RUMC-LT acceleration signals in point 19 of Fig. 5a. a** *X* represents feed direction. **b** *Y* means perpendicular to the feed direction. **c** *Z* is along the axial direction of milling tool.

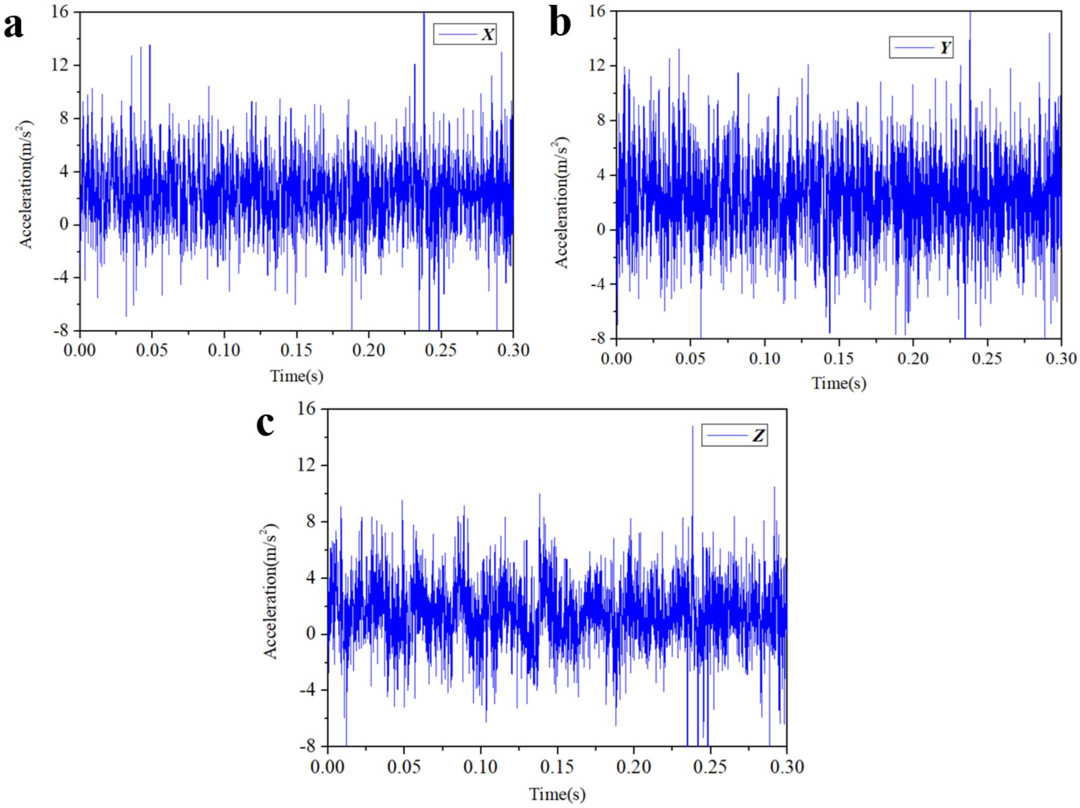


**Supplementary Fig. S26. RUMC-LT acceleration signals in point 20 of Fig. 5a. a** *X* represents feed direction. **b** *Y* means perpendicular to the feed direction. **c** *Z* is along the axial direction of milling tool.

## Supplementary Table S1.

**Supplementary Table S1 Initial posture parameters of industrial robot (KUKA KR500).**

| Joint angle | Value(deg) | Joint angle | Value(deg) |
|---|---|---|---|
| $\boldsymbol{\theta_1}$ | 6.824 | $\theta_4$ | 9.535 |
| $\boldsymbol{\theta_2}$ | -69.368 | $\theta_5$ | -45.796 |
| $\boldsymbol{\theta_3}$ | 114.668 | $\theta_6$ | -6.691 |

**Supplementary Table S2.**

**Supplementary Table S2 Robotic modes in *X*/*Y*/*Z* directions (KUKA KR500).**

| Mode | Natural frequency $p_n$ (Hz) | Damping Ratio $\xi$ (%) | Modal mass $m$ (Kg) | Mass normalized mode shape vector (1/Kg$^{0.5}$) |
|---|---|---|---|---|
| **R1** | 68/60 /72 | 3.53/ 3.78/3.84 | 150.65/193.50/134.37 | 0.44/0.53/0.62 |
| **R2** | 135/217 /227 | 2.08/2.18 /2.53 | 38.22/14.79/13.52 | 0.49/0.58/0.67 |
| **R3** | 304/ 300/339 | 2.66/ 2.85/2.60 | 7.54/7.74/6.06 | 0.33/0.40/0.56 |
| **R4** | 538/ 536/540 | 2.47/1.17 /1.84 | 2.41/2.43/2.39 | 0.51/0.64/0.67 |
| **R5** | 618/728 /715 | 1.31/ 0.95/0.99 | 1.82/1.31/1.36 | 0.31/0.46/0.66 |

## Supplementary Table S3.

**Supplementary Table S3 Modes of component system with low stiffness.**

| **Mode** | **Natural frequency** $p_n$ **(Hz)** | **Damping Ratio** $\xi$ **(%)** | **Modal mass** $m$ **(Kg)** | **Mass normalized mode shape vector** **($1/Kg^{0.5}$)** |
|---|---|---|---|---|
| **C1** | 136 | 2.34 | 1.479 | 9.49/7.59/2.75 |
| **C2** | 324 | 4.82 | 0.261 | 5.72/5.56/6.08 |
| **C3** | 778 | 3.83 | 0.045 | 6.97/6.81/1.22 |

**Supplementary Table S4.**

**Supplementary Table S4 Values of milling force coefficients.**

| Coefficient | Value | Unit |
|---|---|---|
| $K_t$ | 848 | N/mm $^{1+q}$ |
| $K_r$ | 323 | N/mm $^{1+q}$ |
| $K_a$ | 340 | N/mm $^{1+q}$ |
| $q$ | 0.776 | / |

**Supplementary Table S5.**

**Supplementary Table S5 Parameters of robotic posture (KUKA KR210).**

| Coordinate axis | Value(mm) | Rotation axis | Value(deg) |
|---|---|---|---|
| **X** | 1777.41 | A | 165.5 |
| **Y** | 44.25 | B | 0 |
| **Z** | 1547.66 | C | 180 |

**Supplementary Table S6.**

**Supplementary Table S6. Robotic modes in three-coordinate directions (KUKA KR210).**

| Mode | $f_{nx}$/ $f_{ny}$/ $f_{nz}$ (Hz) | $\xi_{nx}$/$\xi_{ny}$/$\xi_{nz}$ (%) | $m_{tx}$/ $m_{ty}$ / $m_{tz}$ (kg) |
|---|---|---|---|
| **R1** | 15/18/10 | 1.82/1.59/2.28 | 180.127/125.088/405.285 |
| **R2** | 85/81/90 | 2.01/2.00/2.37 | 5.609/6.177/5.004 |
| **R3** | 165/185/150 | 2.5/2.34/1.67 | 1.489/1.184/1.801 |
| **R4** | 385/322/452 | 2.11/2.55/1.90 | 0.273/0.391/0.198 |
| **R5** | 720/675/787 | 2.22/1.96/2.50 | 0.083/0.089/0.065 |

**Supplementary Excel S1**

It presents the original calculation results of Supplementary Fig. S2 and Supplementary Fig. S3, which includes the spindle speed and axial cutting depth.

**Supplementary Excel S2**

It consists of three parts. Firstly, there are 30 groups experimental data about the RUMC-LT. Secondly, there are 40 groups data which represents the robotic longitudinal-torsional ultrasonic milling rigid plate (Al7075-T7). Thirdly, there are 30 groups data about robotic longitudinal-torsional ultrasonic milling CFRP. In summary, the 100 groups data denotes the original experiment result in Fig. 5e.

## References


1. Cordes, M., Hintze, W. & Altintas, Y. Chatter stability in robotic milling. *Robot. Cim-Int. Manuf.* **55**, 11-18 (2019).
2. Ahmadi, K. & Altintas, Y. Identification of machining process damping using output-only modal analysis. *J. Manuf. Sci. E-T. ASME.* **136**, 051017 (2014).
3. Wan, M., Dang, X., Zhang, W. & Yang, Y. Optimization and improvement of stable processing condition by attaching additional masses for milling of thin-walled workpiece. *Mech. Syst. Signal. Pr.* **103**,196-215 (2018).
4. Ding, Y., Zhu, L., Zhang, X. & Ding, H. Second-order full-discretization method for milling stability prediction. *Int. J. Mach. Tool. Manu.* **50**, 926-932 (2010).
5. Insperger, T., Mann, B. & Surmann, T. On the chatter frequencies of milling processes with runout. *Int. J. Mach. Tool. Manu.* **48**,1081-1089 (2008).
6. Sun, L. et al. Stability analysis of robotic longitudinal-torsional composite ultrasonic milling. *Chin. J. Aeronaut.***35**, 249-264 (2022).
7. Sun, L. et al. Investigation on chatter stability of robotic rotary ultrasonic milling. *Robot. Cim-Int. Manuf.* **63**, 101911 (2020).
8. Cordes, M., Hintze, W. & Altintas, Y. Chatter stability in robotic milling. *Robot. Cim-Int. Manuf.* **55**, 11-18 (2019).